Geomorphology 183 (2013) 28–44

Contents lists available at SciVerse ScienceDirect

Geomorphology

journal homepage: www.elsevier.com/locate/geomorph

Characterizing spatial variability in velocity and turbulence intensity using 3-D acoustic Doppler velocimeter data in a plane-bed reach of East St. Louis Creek, Colorado, USA

Gabrielle C.L. David [a,*], Carl J. Legleiter [b], Ellen Wohl [c], Steven E. Yochum [d]

[a] Bowdoin College, Department of Earth and Oceanographic Science, Brunswick, ME 04011, USA
[b] University of Wyoming, Department of Geography, Laramie, WY 82071, USA
[c] Colorado State University, Department of Geosciences, Fort Collins, CO 80523, USA
[d] USDA Natural Resources Conservation Service, Fort Collins, CO 80523, USA

ARTICLE INFO

Article history:
Received 2 June 2011
Received in revised form 23 May 2012
Accepted 26 July 2012
Available online 3 August 2012

Keywords:
Stage-dependent flow structure
Semivariogram
Stochastic hydraulics
Plane-bed
Mountain streams
Boulder-bed river

ABSTRACT

We investigated the influence on flow resistance of flow structure and turbulence at the reach scale in a mountain channel using 3-D velocity measurements and geostatistical analysis to understand the complexity of the flow structure in a reach with limited bed irregularities. The increase in flow resistance at low flows in a plane-bed reach was not fully explained by grain resistance, therefore detailed 3-D velocity measurements were made to investigate spatial variability in velocity and turbulence components and potential controls on flow resistance. One plane-bed reach was surveyed over two stages in Fraser Experimental Forest, Colorado, using a combination of a total station, LiDAR (Light Detection and Ranging), and a SonTek Flowtracker handheld ADV (acoustic Doppler velocimeter). LiDAR was used to capture bank and channel geometry at low flows, whereas the water surface and bed data were collected with the total station at all flows. We used the standard deviation of bed elevation (σ_b) within a moving window as an index of roughness height (k_s) and calculated the relative submergence of the bed at different stages as h/k_s, where h is the local flow depth. ADV measurements were collected on a grid with a 0.3 m to 0.5 m spacing. Geostatistical analysis of the velocity data indicated that the flow was highly three-dimensional and varied based on stage, demonstrating that even small irregularities in the bed have a significant influence on the flow characteristics. The streamwise component was the largest at both low and high flow, but varied more throughout the reach at low flow. At high flow, the greatest streamwise velocities were located within the thalweg. Areas of upwelling and downwelling also varied based on stage, with this component being strongly influenced by small changes in the morphology at high flow, and by protuberant grains at low flows. The cross-stream velocity and turbulence components were controlled by the flow structure and less by the roughness of the bed. The turbulence intensity is significant when considering hydraulics for predicting sediment transport and for habitat assessment.

The plane-bed flow patterns were compared to results from a pool-riffle reach in the North Fork Cache La Poudre River, a step-pool reach in East St. Louis Creek, and a step-pool reach in Italy on the Rio Cordon. The comparison of the 3-D velocities among channel types showed that the plane-bed reach has higher streamwise velocities, but similar values of cross-stream and transverse velocities. Streamwise turbulence intensities were similar in both the plane-bed and step-pool reach in East St. Louis Creek. The analysis revealed that the connection between the flow characteristics and the channel was not only related to the gross morphology and location of larger clasts, but also to the development of shear layers from the convergence of flow. Therefore, it is essential to understand how water moving in one direction can alter the characteristics of another component of flow and how this interaction is connected to the bed morphology.

1. Introduction

Velocity and turbulence in stream channels vary spatially and temporally as a function of flow depth, slope, boundary roughness, cross-sectional geometry, bedforms, and sediment load. Many applications–including modeling flows, understanding hydraulic performance for flood conveyance, developing sediment transport

* Corresponding author.
E-mail addresses: gdavid@bowdoin.edu (G.C.L. David), Carl.Legleiter@uwyo.edu (C.J. Legleiter), ellenw@warnercnr.colostate.edu (E. Wohl), steven.yochum@co.usda.gov (S.E. Yochum).

0169-555X/$ – see front matter © 2012 Elsevier B.V. All rights reserved.
http://dx.doi.org/10.1016/j.geomorph.2012.07.026

equations, and restoring and managing river habitat–require information about changes in velocity and turbulence across space and over time (Clifford et al., 2002, 2010; Rhoads et al., 2003; Marchildon et al., 2011). Nonetheless, the flow field is most often summarized in terms of the downstream, depth-averaged component, assuming a logarithmic velocity profile and steady uniform flow (Keulegan, 1938; Bathurst, 1993):

$$\frac{u}{U_*} = \frac{2.303}{\kappa} \log\left[\frac{y}{k_s}\right] + B \quad (1)$$

where, u = velocity (m s^{-1}) at distance y (m) above the bed; U^* = shear velocity (m s^{-1} ($\sqrt{gRS_f}$, g is acceleration due to gravity, R is hydraulic radius, S_f is the friction slope); κ = the von Kármán constant; B = a constant which depends on bed characteristics; and k_s a measure of bed roughness (m). Eq. (1) can be useful for modeling flow in low-gradient systems, but is less appropriate where velocity profiles tend to be s-shaped or highly irregular as flow moves over coarser clasts in high-gradient channels (Wiberg and Smith, 1991; Byrd et al., 2000; Lawless and Robert, 2001). Mountain streams have more complex flow structures, with sediment grain sizes on the same order as the flow depth, step-pool bed morphology, and inputs of wood and boulders from adjacent hillsides.

Velocity in steep, coarse-grained streams is dominated by flow separation, wakes, and vortex shedding as the flow is affected by larger objects and bedforms (Roy et al., 1999; Thompson, 2007). Turbulence is characterized by the interactions among flow structures of various sizes and origins, which cause fluctuations in streamwise, vertical, and transverse velocity components (Roy et al., 1999). Turbulence, which results in bursts and sweeps, is related to changes in drag and lift forces that act to transport sediment (Nelson et al., 2001). The average boundary shear stress and time-averaged velocity do not characterize turbulence structure and, therefore, are inappropriate for predicting sediment transport (McLean et al., 1994; Nelson et al., 1995).

Macroturbulent flow structures are an important component of flow in coarse-grained channels. For example, oblique high- and low-speed wedges are associated with the formation of vortices and bursts of low momentum fluid toward the surface and sweeps of high momentum fluid toward the bed (Ferguson et al., 1996; Buffin-Belanger et al., 2000; Roy et al., 2004). Flow separation around protuberant clasts or bedforms causes recirculation on the lee side of an object, which creates eddies that are shed into the flow field. The shedding structures then create slow flow which emerges from the bed and moves toward the water surface (Lamarre and Roy, 2005).

Macroturbulent flow structures depend on bed roughness and hydraulic conditions – the larger the flow depth and velocity, the better-developed the coherent flow structure (Shvidchenko and Pender, 2001; Hardy et al., 2009). At higher discharges, macroturbulent flow structures can, thus, form independently of localized roughness and remain organized over the reach scale, even in coarser-grained cobble-bed channels (Lamarre and Roy, 2005; Legleiter et al., 2007; Noss et al., 2010). In general, these larger-scale structures result from flow-bed interactions, whether gross morphology or individual roughness elements, and dissipate as they move upward through the flow depth.

As macroturbulent structures become more defined as discharge increases, flow resistance generally decreases and velocity increases in all types of channels (Bathurst, 1993; Comiti et al., 2007; Reid and Hickin, 2008; David et al., 2010a,b). Flow resistance is related to skin friction and form drag around bedforms, protuberant clasts, and in-channel wood (Leopold et al., 1960; Wilcox and Wohl, 2006; David et al., 2010a) and varies based on flow stage, gradient (Lee and Ferguson, 2002; Ferguson, 2007; Reid and Hickin, 2008; David et al., 2010b, 2011), and macroturbulent flow structure (Roy et al., 1999). Flow resistance can be related to the velocity profile by (Ferguson, 2007):

$$\frac{U}{U_*} = \sqrt{\frac{8}{ff}} \quad (2)$$

where U = mean velocity in the streamwise direction (m s^{-1}); ff = Darcy–Weisbach friction factor. The use of reach-average velocities makes it difficult to distinguish different types of flow resistance such as grain, form and spill (David et al., 2011).

The majority of previous work on spatial and temporal variation in velocity and turbulence has been done in lower-gradient, gravel-bed, pool-riffle channels. Relatively few studies have attempted to characterize flow structure in steeper channels. High-gradient mountain streams (S_0 > 0.01 m/m, where S_0 = gradient) are characterized by three distinct channel morphologies: step-pools (0.03 < S_0 < 0.10 m/m), cascades (S_0 > 0.06 m/m) and plane-beds (0.01 < S_0 < 0.03 m/m) (Montgomery and Buffington, 1997). Step-pools have alternating plunging supercritical flow over steps and subcritical flows in the pools below, while cascades are characterized by tumbling flow over large, randomly arranged clasts (Montgomery and Buffington, 1997; Zimmerman and Church, 2001; Church and Zimmerman, 2007). Plane-bed channels have a uniform topography and lack any regular bedforms (Montgomery and Buffington, 1997; Chartrand and Whiting, 2000). Here, the term plane-bed applies to an armored cobble-bed channel, which occurs at moderate to high gradients, and should not be confused with a planar bed phase described for upper regime flows in a sand-bed channel (Montgomery and Buffington, 1997).

A number of previous studies have focused on spatially explicit description of velocity in step-pool channels (Wilcox and Wohl, 2007; Wilcox et al., 2011), but relatively little effort has been directed toward understanding plane-bed reaches in high-gradient cobble and boulder bed systems. By definition, plane-bed reaches do not have the regular geometry of a step-pool channel or the highly irregular structure of a cascade reach. Therefore, little is known about their spatial structure; these reaches are simply assumed to be uniform, with no spatial organization. Legleiter et al. (2007) found that a spatially explicit, geostatistical description of the flow field was essential for understanding the effects of stage and roughness on velocity and turbulence characteristics across a single riffle, which can be considered analogous to a plane-bed reach. Therefore, the objectives of this paper are to i) understand how flow structure varies as a function of flow stage within a plane-bed channel by examining spatial patterns of downstream, vertical, and cross-stream velocities and turbulence intensities at two different discharges; ii) determine how bed roughness (h/k_s, where h is the flow depth and k_s is a representative roughness height) affects flow structure during both high (close to bankfull) and low (baseflow) discharges; and iii) compare the magnitudes and spatial patterns of individual velocity components observed along a plane-bed reach with similar data from pool-riffle and step-pool channels.

2. Methods

2.1. Field methods

Detailed velocity measurements were obtained from a plane-bed channel at two different discharges using an acoustic Doppler velocimeter (ADV). These data were collected along a 6.5 m reach of East St. Louis Creek (ESL) located in Fraser Experimental Forest, in the Rocky Mountains 112 km west-northwest of Denver, Colorado (Fig. 1). The elevation of the study reach is 2927 m, with an approximate drainage area of 8.73 km^2. Runoff is dominated by snowmelt during the summer months with small contributions from summer convective storms. Average annual precipitation over the entire forest is 787 mm (USDA Forest Service, 2009).

Measurements were made at a high flow during the 2008 spring runoff period (June 13) and again at base flow (August 20) after the snowmelt had receded (Table 1 and Fig. 2). The high flow remains within the channel, but is close to filling the channel to the top of the banks. Bed topography was measured using a total station and a

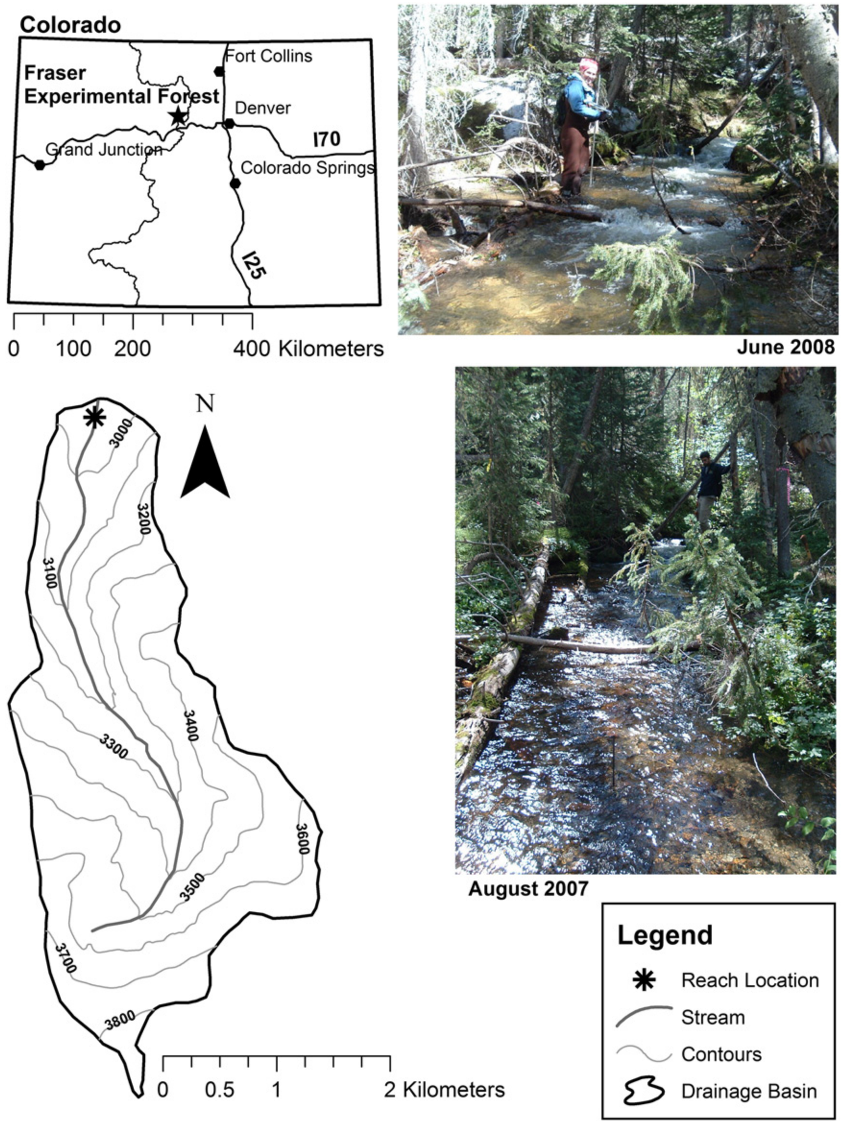

Fig. 1. Map showing the location of Fraser Experimental Forest in Colorado and the location of the plane bed reach on East St. Louis Creek. Photographs are shown of ESL during high (June 2008) and low (August 2007) flows. The August 2007 flow is at a similar stage as the August 2008 flow with the downstream gage reading at 0.10 $m^3\ s^{-1}$ in August 2007 and at 0.12 $m^3\ s^{-1}$ during August 2008.

ground-based LiDAR scanner was used to survey wood and large clasts that protruded above the low-flow water surface (Fig. 3). Although the reach is described as plane-bed, it does have some small features, including a bed irregularity in the center of the reach that creates a small step (~0.07 m). One log crosses the channel and creates a small hydraulic jump during high flows, but was not submerged during the low flow measurements (Fig. 1). The upper part of the reach features several protruding boulders with diameters averaging about 300 mm. These boulders can be seen as distinct objects in the middle part of the channel in Fig. 3 and are shown as irregular shapes in the channel on the contour maps (Fig. 4). For the remainder of the bed material, the grain size distribution was characterized by performing a Wolman (1954) pebble count consisting of 300 pebbles. Grain size is in the cobble range, with D_{50} and D_{84} particle sizes of 20 mm and 85 mm, respectively. Additional detail on the survey methods used in this study is available in David et al. (2010a).

Three-dimensional velocity measurements were made with a SonTek FlowTracker ADV (SonTek, 2001). These data were collected on a regular grid with along- and across-channel spacing of 0.3 to 0.5 m between measurements. The location of each point was surveyed using a total station prior to the velocity measurement, and velocity data were recorded at 0.6 h below the water surface, where h is the local flow depth. The ADV measures velocity based on the Doppler frequency shift between emitted acoustic pulses and their reflection from material suspended within a small sampling volume (Lane et al., 1998) located a fixed distance (10 cm) from a probe mounted on a top-setting wading rod. The ADV resolves the instantaneous velocity vector into streamwise, vertical, and cross-stream velocities, denoted as u, v, w, respectively. Table 2 indicates the notation for each velocity component. 180 s time series were recorded at a frequency of 1 Hz for each location. Although a shorter sampling duration (60–90 s) might be sufficient for higher frequency instruments (Buffin-Belanger and Roy, 2005), a longer sampling duration was selected for the lower frequency FlowTracker. In this paper, we focused on time-averaged, reach-scale spatial patterns of velocity and turbulence rather than coherent flow structures or bursts or sweeps. The 1 Hz sampling frequency would be an important instrumental limitation

Table 1
Summary of reach-average values of each variable for June and August 2008.

Date	Q	A	R	h	S_w	k_s	h/k_s	U	V	W	ff
	$m^3\ s^{-1}$	m^2	m	m		m		$m\ s^{-1}$	$m\ s^{-1}$	$m\ s^{-1}$	
June 13, 2008	0.431	0.63	0.20	0.254	0.0219	0.039	7.79	0.730	0.022	0.034	0.64
August 20, 2008	0.116	0.37	0.13	0.136	0.0205	0.034	4.68	0.432	0.010	0.052	1.12

Q = Discharge; A = Cross-sectional area; R = Hydraulic Radius; h = Flow depth; S_w = reach-averaged water surface slope; k_s = roughness height; h/k_s = relative roughness; U = average downstream velocity; V = average vertical velocity; W = average cross-stream velocity; ff = Darcy–Weisbach friction factor.

for more detailed turbulence studies (Soulsby, 1980), but the relatively low sampling frequency was not problematic for our analysis of time-averaged mean velocities and turbulence intensities (Legleiter et al., 2007).

2.2. Data analysis

The FlowTracker is susceptible to error related to obstructions in or near the sampling volume, excessive aeration, and data collection near the water surface, particularly in coarse-grained mountain streams (MacVicar and Roy, 2007; Wilcox and Wohl, 2007). The data were filtered prior to calculation of flow statistics using the methods described in Legleiter et al. (2007). Typically, only 1–2% of the velocity time series from any given measurement location was filtered and replaced by interpolated values, and in no case did the proportion of the time series replaced by interpolated data exceed 20%.

Survey data from both flow measurement periods were combined and used to characterize the bed topography, which did not change during the time interval between the June and August field campaigns. Even during the near-bankfull flows observed in June, the bed material was not mobile, and this lack of movement indicates that higher, possibly overbank, flows would be required to entrain significant amounts of sediment and alter the morphology of the channel. In total, 738 points were recorded and used to obtain a continuous topographic representation of the channel by kriging with a trend (Legleiter and Kyriakidis, 2008). Both flow measurements and survey points were transformed to the *s*-*n*-*z* coordinate system described in Table 2 using the method outlined in Legleiter and Kyriakidis (2008). The original survey points were also used to calculate a roughness height (k_s) as the standard deviation of the bed elevations, σ_b, within a moving window that extended 1 m upstream, 0.25 m downstream, and 0.25 m to either side of each velocity measurement location. These resulting k_s values were then used to calculate the relative submergence as h/k_s, where h is the local flow depth. Because a local measure of roughness was necessary to characterize connections between local boundary roughness and point measurements of velocity, we used σ_b within a neighborhood centered on each ADV measurement position rather than a reach average grain size (Aberle and Smart, 2003; Ferguson, 2007). Previous studies have shown that the relative submergence using σ_b better characterizes the roughness of the bed in high-gradient channels than does reach average grain size (David et al., 2010a; Coleman et al., 2011; Yochum et al., 2012). Sensitivity analysis of the effect of window size on σ_b indicated that halving, doubling, or even quadrupling the size of the local neighborhood within which bed elevations were pooled to calculate σ_b did not result in significant differences in mean relative submergence values for this channel.

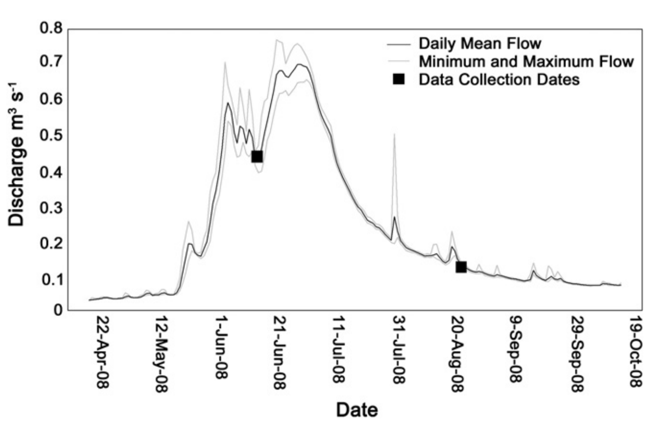

Fig. 2. The 2008 hydrograph of East St. Louis Creek showing minimum, maximum and mean daily flows. The high and low flow ADV data collection days are indicated on the figure.

To facilitate comparison of the two discharges, the flow field at each discharge was characterized in terms of non-dimensional mean velocities and turbulence intensities. The instantaneous velocity data were first decomposed into time-averaged mean (U, V, W) and fluctuating components, with the latter representing deviations from the time average. Turbulence intensities (u', v', w') were obtained by computing the root mean square values from the filtered ADV time series (Clifford and French, 1993). Both velocity and turbulence intensity were non-dimensionalized by dividing the values by the shear velocity, defined as $U_* = \sqrt{g\bar{h}S_W}$, where g is gravitational acceleration, $\bar{h}$ is reach-average flow depth, S_w is reach-averaged water surface slope. All water surface elevation data during each measurement period were used to calculate an average water surface slope. The water surface elevation was determined by using the surveyed bed elevations and adding the measured flow depth. The slope was calculated by using a regression of all water surface elevation points against the streamwise coordinates of the points. Scaling the data by shear velocity enabled a comparison between low and high flows for which the mean depth and water surface slope were different (Table 1).

To visualize the spatial structure of the flow field and understand how the bed topography influenced the flow at different discharges, the non-dimensionalized velocity and turbulence intensity data were plotted as proportional symbols on a contour map of the channel (Fig. 4a). The minimum surveyed elevation of the bed was set to zero and used as a vertical datum for the bed topography. Fig. 4 gives a general description of how to interpret the contour maps, histograms, and semivariograms in the subsequent figures. The maps show the location of each ADV measurement and represent the value of the non-dimensional velocity component at that location. The symbol size and color are both scaled to the deciles of the pooled distribution (i.e., combining both high- and low-flow observations) of each variable, so that a larger symbol indicates larger values for the downstream component (U/U_*), for example. The symbols that represent the vertical component of velocity encompass both directions, with large symbols for upwelling and smaller symbols for downwelling. Lastly, the symbols for the transverse component are split between large highlighted circles indicating flow moving in the positive n direction towards the left bank, or smaller highlighted circles

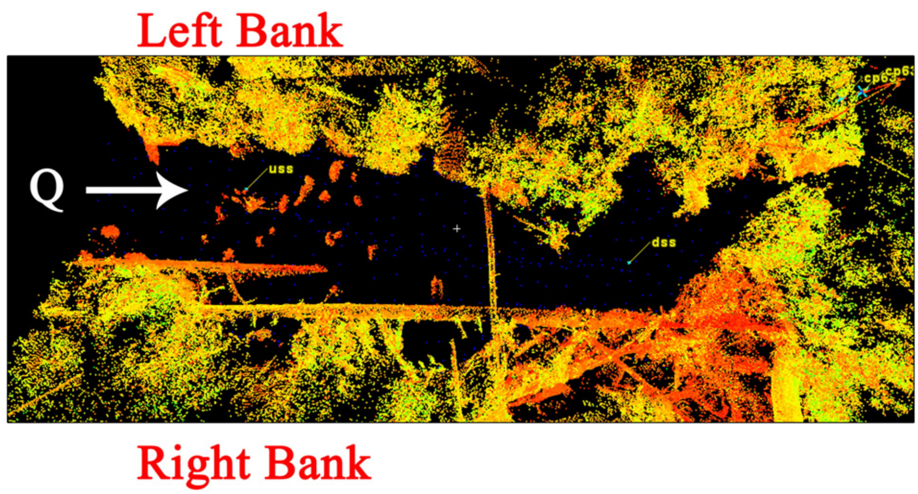

Fig. 3. Plan view of LiDAR scan. The arrow shows the direction of flow and the left and right banks are labelled.

indicating flow moving in the negative *n* direction towards the right bank. As a result, the size of the symbols in the maps for the vertical and transverse components does not necessarily directly correspond to the magnitude of the non-dimensional flow, because positive or negative indicate direction and the values are not necessarily symmetric about 0.

These non-dimensional data were used to examine and quantify spatial patterns of velocity and turbulence intensity by means of two geostatistical metrics of spatial structure, the semivariogram and correlogram (Fig. 4c). This analysis was similar to that performed in a previous study of a pool-riffle channel, and additional detail

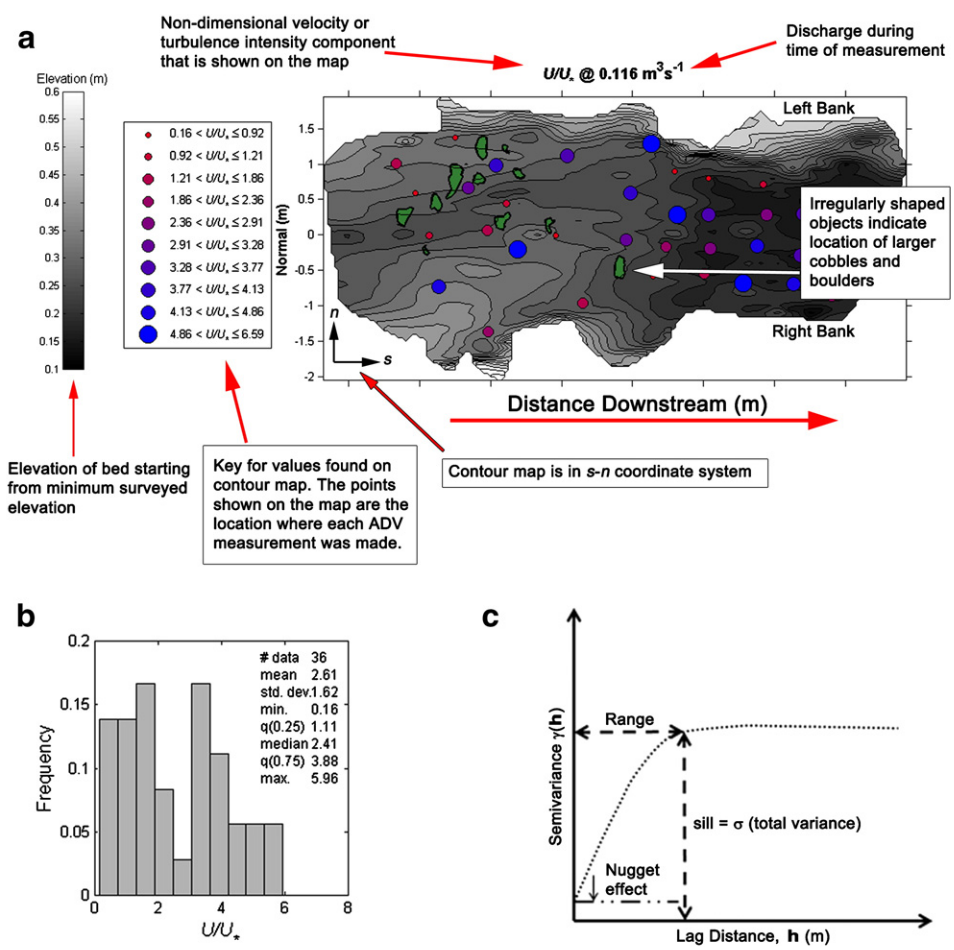

Fig. 4. Example with explanation of the (a) proportional symbol maps, (b) probability density histograms, and (c) semivariograms that are used to analyze each non-dimensional component of velocity and turbulence. The contour maps (a) are in the *s*–*n* coordinate system with flow moving downstream towards the right of each map and the positive *n* direction toward the left bank at the top of the map. The probability density histograms (b) show the distribution of each velocity component depicted in the corresponding map, along with some summary statistics. The semivariogram (c) shows the horizontal asymptote, or sill, beyond which the points are no longer correlated. The sill represents the a priori variance. The range is the distance at which the semivariance approaches the sill. A vertical offset [i.e., $\gamma(\varepsilon)>0$, where ε is a very small lag distance] on such a plot represents fine-scale variations not captured by the sampling strategy and/or random measurement error and is referred to as a nugget effect (Goovaerts, 1997).

Table 2
Notation for measured and calculated velocity components.

Direction	Downstream	Vertical	Cross-stream
Coordinate	s	z	n
Time-averaged mean velocity (m s^{-1})	U	V	W
Positive direction	Downstream	Upward	Left bank
Fluctuating velocity (m s^{-1})	u	v	w
Turbulence intensity (root mean square velocity; m s^{-1})	u'	v'	w'
Non-dimensional mean velocity	U/U_*	V/U_*	W/U_*
Non-dimensional turbulence intensity	u'/U_*	v'/U_*	w'/U_*

regarding the geostatistical methodology is available in Legleiter et al. (2007). Briefly, the semivariogram is defined by Eq. (3):

$$\gamma(\mathbf{h}) = \frac{1}{2N(\mathbf{h})}\sum_{\alpha=1}^{N(\mathbf{h})}\left[z(x_\alpha) - z(x_\alpha + \mathbf{h})\right]^2 \quad (3)$$

where $\mathbf{h}$ = lag vector separating pairs of observations of the random variable z at locations given by x_α and $x_\alpha + \mathbf{h}$, and $N(\mathbf{h})$ is the number of pairs with separation vectors encompassed by a specified range of distances and directions centered about $\mathbf{h}$ (Goovaerts, 1997). In this study, the semivariance was used to evaluate the degree of spatial dependence between observations of either non-dimensionalized velocity or non-dimensionalized turbulence intensity as a function of the distance between observations, both along and across the channel. As the lag ($\mathbf{h}$) increases, observations of velocity and turbulence intensity tend to become less strongly correlated with one another, such that the mean difference between pairs of observations becomes larger, resulting in larger values of $\gamma(\mathbf{h})$. Beyond a certain separation distance, pairs of observations are no longer spatially correlated with one another and the mean squared difference between pairs of observations separated by such large lag distances will be equal in magnitude to the a priori variance of the data set (the sill). The distance at which the semivariance approaches the sill is called the range (Fig. 4c). The sill and range of a semivariogram, thus, provide information on the magnitude of velocity variation and the characteristic spatial scale over which this variation occurs. Fitting a parametric model to the observed semivariance values, thus, yields a concise summary of the spatial structure of the attribute. In this study, Gaussian and exponential models with sill, range, and nugget parameters were fitted to the velocity and turbulence intensity semivariograms using an iterative graphical and weighted least squares routine, as described by Legleiter et al. (2007). Whereas Legleiter et al. (2007) fitted separate models for the streamwise and transverse directions, in this study both directions were considered simultaneously and a single anisotropic model, applying to both directions, was fitted. The nugget parameter was held fixed at the initial, by-eye estimate because of numerical instability in the fitting routine when the nugget was allowed to vary.

A similar but multivariate geostatistical metric, the cross-correlogram, was used to compare the spatial covariance between the non-dimensionalized velocity and turbulence intensities and the relative roughness of the bed. The cross-covariance between two random variables z_i and z_j at opposite ends of the vector $\mathbf{h}$ was calculated with Eq. (4):

$$C_{ij}(\mathbf{h}) = \frac{1}{N(\mathbf{h})}\sum_{\alpha=1}^{N(\mathbf{h})} z_i(x_\alpha)\cdot z_j(x_\alpha + \mathbf{h}) - m_{i,-\mathbf{h}}\cdot m_{j,+\mathbf{h}} \quad (4)$$

where, $m_{i,-h} = \frac{1}{N(\mathbf{h})}\sum_{\alpha=1}^{N(\mathbf{h})} z_i(x_\alpha)$ and $m_{j,+\mathbf{h}} = \frac{1}{N(\mathbf{h})}\sum_{\alpha=1}^{N(\mathbf{h})} z_j(x_\alpha + \mathbf{h})$ are means of the z_i value at the tail of $\mathbf{h}$ and the z_j value at the head of $\mathbf{h}$ (Goovaerts,

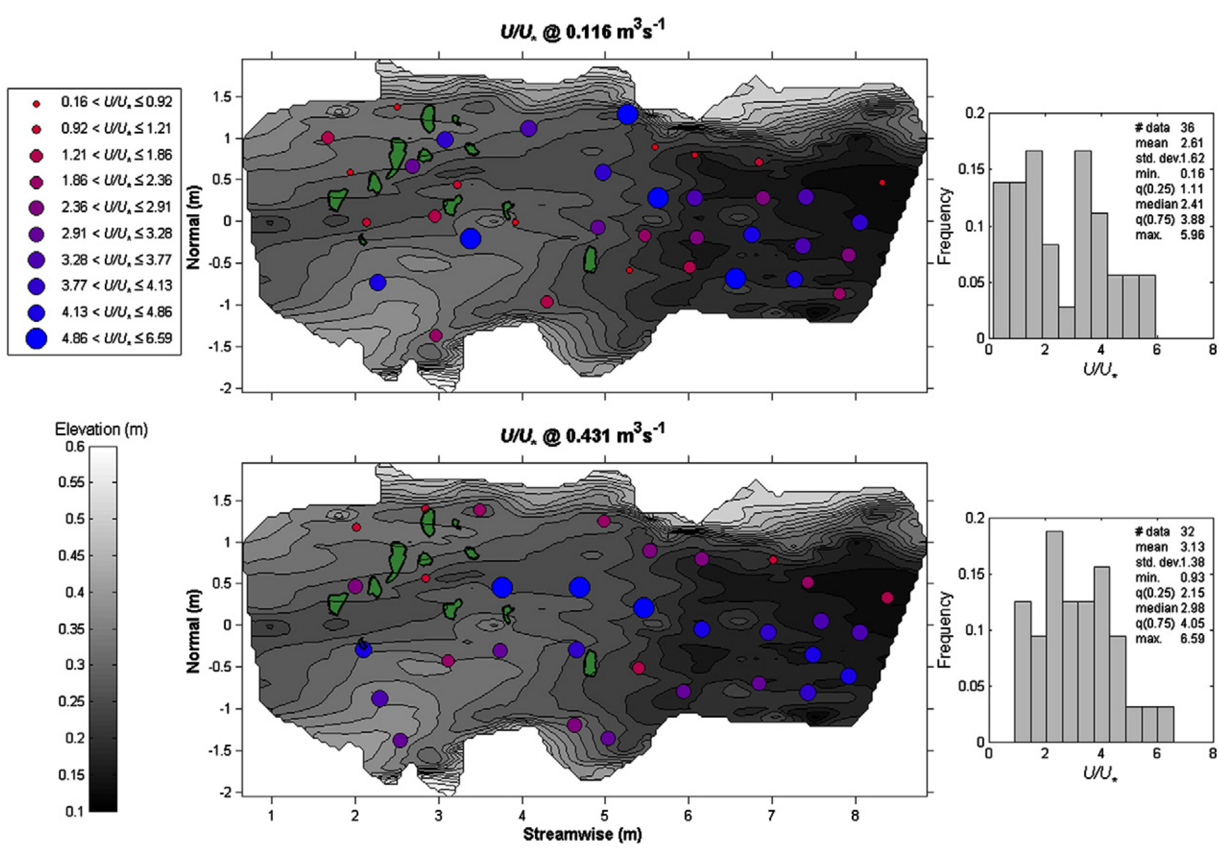

Fig. 5. Proportional symbol map and probability density histograms at each discharge of non-dimensional streamwise velocity (U/U_*).

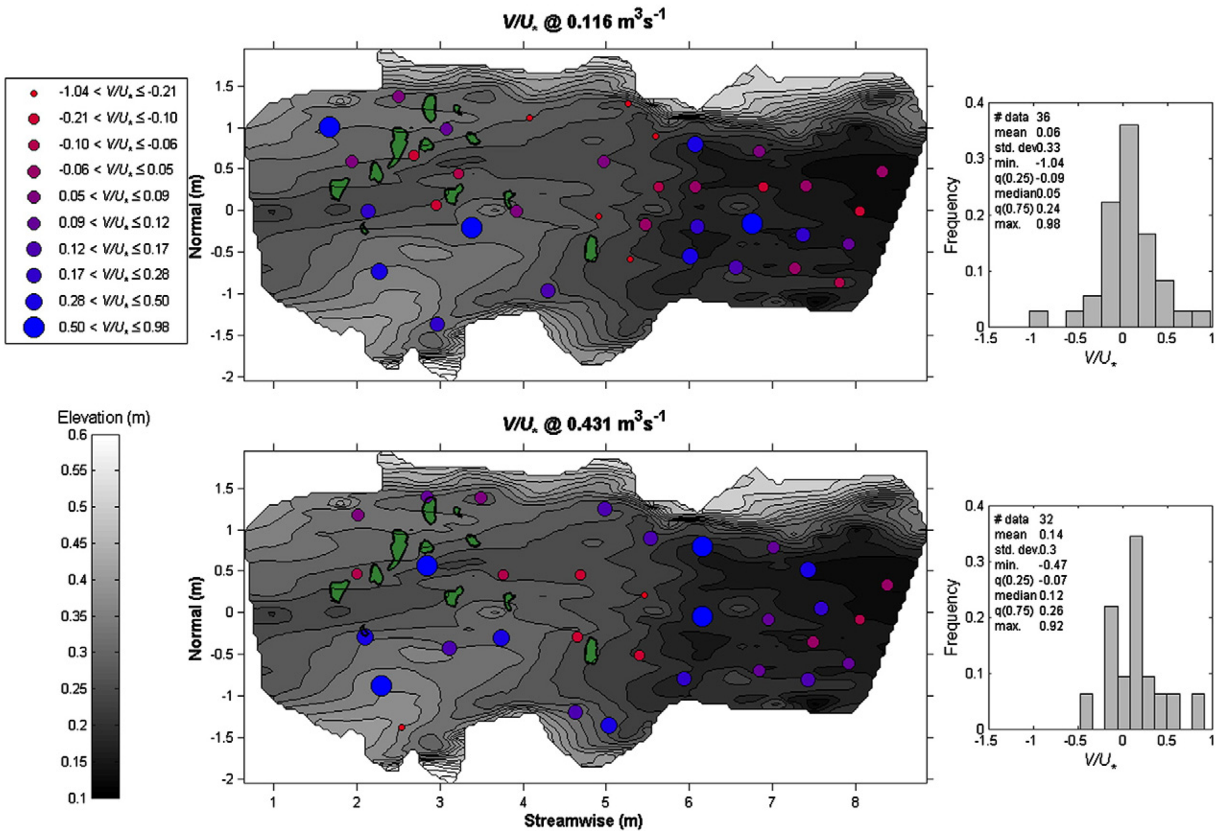

Fig. 6. Proportional symbol map and probability density histograms at each discharge of non-dimensional vertical velocity (V/U_*).

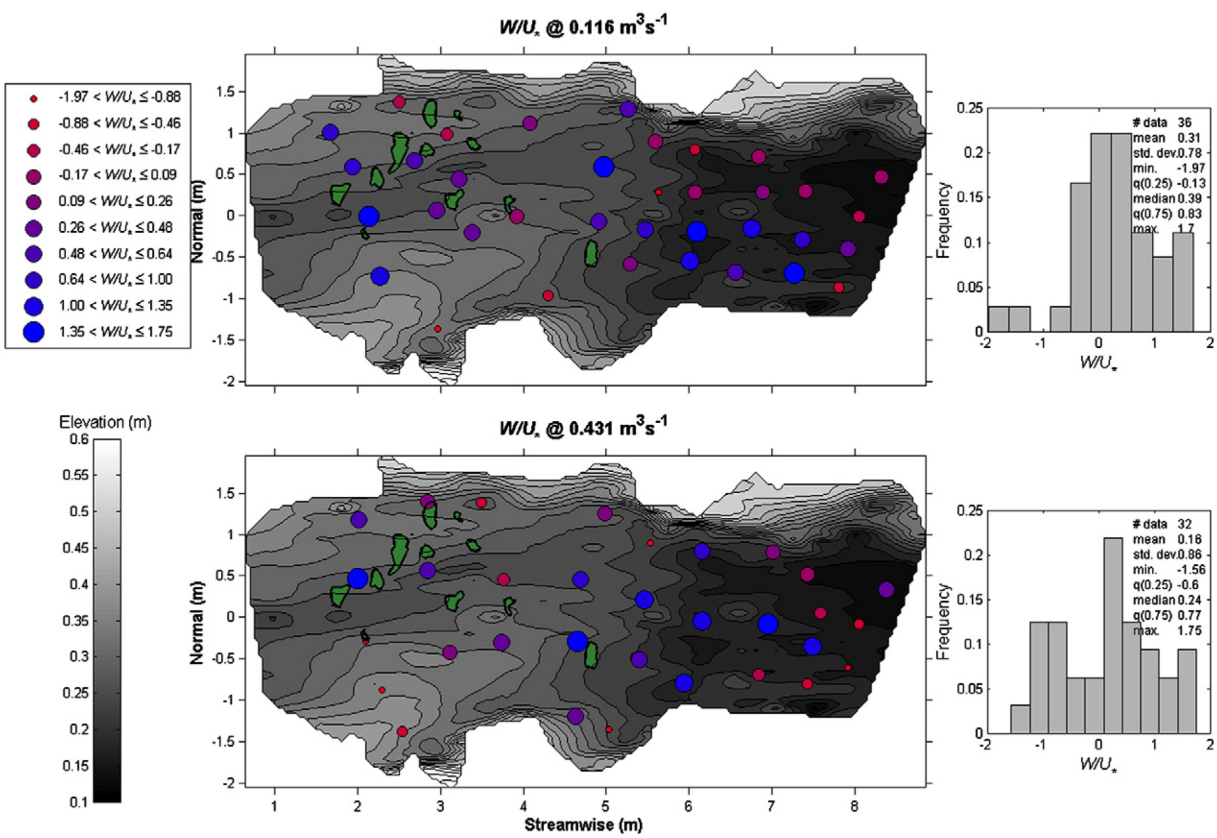

Fig. 7. Proportional symbol map and probability density histograms at each discharge of non-dimensional transverse velocity (W/U_*).

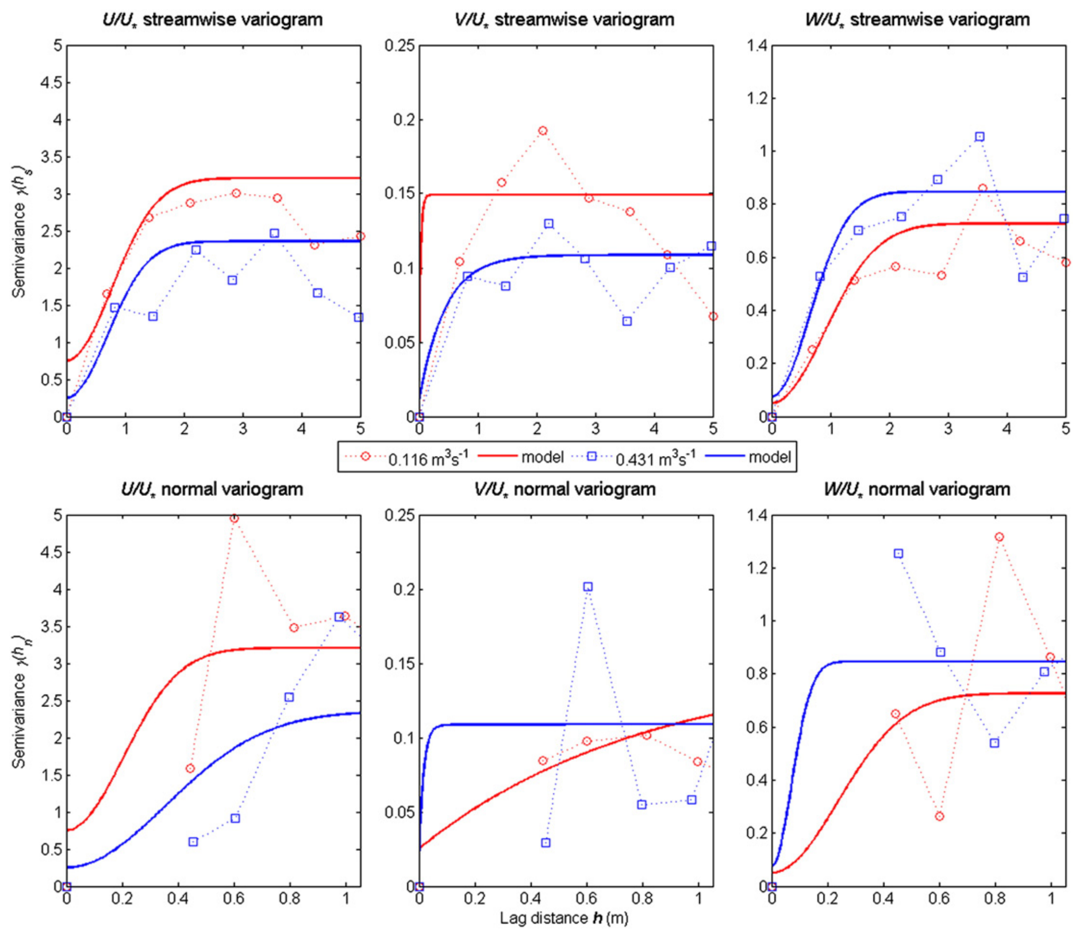

Fig. 8. Semivariograms of non-dimensional velocity in the streamwise and transverse (normal) directions at low (red/circles) and high (blue/squares) flow.

1997). Eq. (5) was used to obtain a more readily interpretable, bounded measure called the cross-correlogram:

$$\rho_{ij}(\mathbf{h}) = \frac{C_{ij}(\mathbf{h})}{\sqrt{\sigma^2_{i,-\mathbf{h}} \cdot \sigma^2_{j,+\mathbf{h}}}} \in [-1, +1] \tag{5}$$

where, $\sigma^2_{i,-\mathbf{h}} = \frac{1}{N(\mathbf{h})}\sum_{\alpha=1}^{N(\mathbf{h})}\left[z_i(s_\alpha) - m_{i,-\mathbf{h}}\right]^2$, $\sigma^2_{i,+\mathbf{h}} = \frac{1}{N(\mathbf{h})}\sum_{\alpha=1}^{N(\mathbf{h})}\left[z_i(s_\alpha + \mathbf{h}) - m_{j,+\mathbf{h}}\right]^2$ are the variances of the tail and head variables z_i and z_j, respectively. Because the magnitudes of z_i and z_j can have different scales, interpreting the cross-covariance defined by Eq. (4) can be difficult. Eq. (5), however, indicates that the cross-correlogram is bounded between −1 and 1. In this study, cross-correlograms quantify the cross-correlation between each flow attribute and relative roughness as a function of distance downstream and across the channel. This analysis thus yielded insight on the local and lagged effects of boundary roughness on the flow field.

3. Results

Our results indicate that the three components of non-dimensional velocity and turbulence intensity vary as a function of flow stage and that this variability is not adequately described by reach-aggregated summary statistics such as means and standard deviations that do not take into account the spatial locations of the data (Figs. 5 to 8; Tables 3 and 4). The 3-D velocity components are shown individually in Figs. 5–7 and their spatial structure is summarized in the semivariograms shown in Fig. 8, with model parameters listed in Table 3, and the results summarized in Table 4. The results are separated into four main sections that correspond with the three goals outlined in the introduction: i) investigate how each velocity component varies with stage and the connection between each of these components and the morphology of the channel (Section 3.1); ii) similarly, investigate the relationship between the turbulence components and flow stage (Section 3.2); iii) investigate the relationship between each velocity component and the relative submergence of the bed (h/k_s); and iv) compare the 3-D velocity components on the plane-bed reach with measurements from a pool-riffle reach in Colorado, a step-pool reach on ESL, and a step-pool reach in Italy, each chosen for the existence of analogous data collected with the same ADV instrument.

3.1. Changes in 3-D velocity components with stage

The velocity component with the greatest magnitude was in the streamwise direction for both low and high discharges, with values ranging from 0.16 to 6.59 (Fig. 5). The mean streamwise velocity (U/U_*) did not vary significantly between low and high flow (2.61 vs. 3.13), but the shape of the histogram (Fig. 5) and the spatial distribution of the streamwise velocity (Fig. 8 and Table 3) differed between the two stages. The variance, shown by the value of the sill in Fig. 8 and Table 3, was greater at low flow than at high flow (2.457 vs. 2.106). The streamwise range parameter was only slightly longer for low flows, a difference of 0.19 m, indicating that the streamwise velocity had a similar downstream spatial correlation length scale at low and high flows. In the transverse direction, the spatial correlation between observations of streamwise velocity was more difficult to interpret because there was more variability, although the variance was

Table 3
Semivariogram model parameters for each flow characteristic at each discharge.

Flow characteristic	Model parameters	Discharge ($m^3 s^{-1}$)	
		0.116	0.431
U/U_*	Nugget	0.75	0.25
	Model type	Gaussian	Gaussian
	Sill	2.457	2.106
	Streamwise range (m)	1.886	1.696
	Transverse range (m)	0.495	0.868
V/U_*	Nugget	0.025	0.010
	Model type	Exponential	Exponential
	Sill	0.124	0.099
	Streamwise range (m)	0.087	1.330
	Transverse range (m)	2.426	0.047
W/U_*	Nugget	0.05	0.075
	Model type	Gaussian	Gaussian
	Sill	0.677	0.772
	Streamwise range (m)	2.197	1.588
	Transverse range (m)	0.578	0.174
u'/U_*	Nugget	0.05	0.005
	Model type	Exponential	Gaussian
	Sill	0.092	0.319
	Streamwise range (m)	3.329	3.132
	Transverse range (m)	1.848	0.515
v'/U_*	Nugget	0.02	0.02
	Model type	Exponential	Exponential
	Sill	0.437	0.856
	Streamwise range (m)	2.310	9.830
	Transverse range (m)	1.866	0.107
w'/U_*	Nugget	0.005	0.0025
	Model Type	Gaussian	Gaussian
	Sill	0.029	0.080
	Streamwise range (m)	2.646	4.772
	Transverse range (m)	0.987	0.216

the same because these anisotropic models were fit by considering the streamwise and transverse directions simultaneously (Fig. 8). The number of measurement locations across the stream might not have been sufficient to obtain reliable estimates of semivariances in the transverse direction, indicating that caution should be used in interpreting the transverse (normal) semivariograms.

During high flows, a clear thalweg was present in the center of the channel and this region features the largest values of U/U_* (Fig. 5). The well-defined thalweg resulted in a longer transverse range for the semivariogram model (Fig. 8 and Table 3). U/U_* was more uniform both in the streamwise and transverse directions at high flow, which was indicated by the reduced variance (Fig. 8 and Table 3). At low flows there was greater variance in U/U_*, with much smaller streamwise velocity near the banks (Fig. 5). A decrease in stage disrupted the obvious thalweg, particularly in the upper portion of the reach where larger clasts distributed over the bed increased the local boundary roughness. The reduced range in the semivariograms for U/U_* in the transverse direction further supports this observation (Fig. 8 and Table 3). The greater variance of U/U_* in the downstream and transverse directions at low flow suggests that localized, even grain-scale, changes in the bed have a more significant effect on the velocity at the lower discharge, although similar streamwise range parameters indicate that other, larger-scale characteristics of the reach influenced the flow structure at both low and high flows.

The vertical (Fig. 6) velocity components (V/U_*) had a smaller range in non-dimensionalized values (-1.04 to 0.98) with a slightly higher mean (0.14 vs. 0.06) at high flow, indicating an increased tendency towards upwelling at high flows (large highlighted circles). The vertical velocity proportional symbol map (Fig. 6) did not indicate a strong dependence on flow stage for either flow, but the semivariograms showed that there was some spatial correlation between points aligned in the streamwise direction at high flow (Fig. 8). In the transverse direction, the model for the vertical velocity component at high flow was essentially a pure nugget effect, implying that there was no cross-stream spatial dependence between points. The proportional symbol map indicated a greater tendency towards downwelling (small highlighted circles) in the center and lower portions of the channel. This downwelling occurred where the bed goes over a lip and becomes steeper at the lower end of the reach. The flow appeared to be directed downward over this convexity in the profile and subsequently upwells with small vertical velocities after the break in slope through the remainder of the reach. The tendency toward downwelling and upwelling around this convexity did not vary with stage. V/U_* was not significantly different between the thalweg and banks at either low or high flows. Fig. 8 and Table 3 indicated that there was little coherent spatial relationship for the vertical velocity component in the transverse direction.

Velocity in the cross-stream (W/U_*) direction (Fig. 7) also had values that span zero (-1.97 to 1.75) as water moves towards the left and right banks in a roughly equal proportion of the measurement locations. The variance for W/U_* exhibited an opposite pattern from that of U/U_* and V/U_*, with the highest variance at the high flow (Fig. 8 and Table 3). The spatial correlation length scale (range) in the streamwise direction was similar for W/U_* and U/U_*, with ranges approaching 2 m at the lowest flow and 1.6 m at the highest flow. The proportional symbol map indicated a strong tendency for the flow to move towards the left bank in the thalweg at the highest flow, with W/U_* being reduced near both banks. The variability in the magnitude and orientation of the transverse velocity near the banks (Fig. 7) accounted for the higher variance in W/U_* in the streamwise direction seen in Fig. 8. At low flow, the lower half of the reach was split, with the flow on the right having a strong transverse flow towards the left bank and the flow on the left having a strong transverse flow towards the right bank, indicating convergence towards the channel center from either bank. This pattern resulted in reduced variability in the streamwise direction (Fig. 8). Although the variance was much smaller for W/U_* versus U/U_*, the spatial correlation length scale (range parameter) was similar (Fig. 8).

3.2. Changes in turbulence intensity with stage

The distribution of turbulence intensities shown in Figs. 9 through 11 sheds further light on how flow stage and bed roughness affected the flow field. The spatial statistics are summarized in Fig. 12, Tables 3 and 4. Overall, the variances (i.e., sill parameters Fig. 12 and Table 3) for the turbulence intensities were much lower than the variances for the mean velocity components. For all three flow components, the streamwise range parameters for the turbulence intensity semivariograms were much greater at high flow (Fig. 12 and Table 3). The proportional symbol maps and semivariograms (Fig. 12) highlight more pronounced differences in the spatial structure of the flow between the two discharges. At high flow, the streamwise turbulence intensity was highest in the thalweg and lowest near the banks and at the lower end of the reach where the grain size was the smallest. The contrast in streamwise turbulence intensity between the upper and lower portions of the reach was expressed as a higher sill in the semivariogram model at high flow. At low flow, the streamwise turbulence intensity was more uniform throughout the reach, resulting in a lower sill for the semivariogram at this discharge.

The vertical turbulence intensity (v'/U_*) (Fig. 10) was much higher in proximity to the larger clasts in the upstream section of the channel, most notably at high flows. Otherwise, during high flows, v'/U_* was much lower in the downstream section of the reach than during the low flow. The semivariograms (Fig. 12) indicated a larger range over which the values are spatially correlated at the higher discharge. The vertical turbulence intensities reached much larger overall values (max = 4.02) than the streamwise (max = 2.76) or transverse (max = 1.15) turbulence intensities, with higher mean values during low flow (Fig. 10).

Table 4
Summary of results for each velocity and turbulence intensity components.

Velocity component	Summary statistics		Semivariogram results			Cross-correlogram results	Other observations
	Means for low and high flow	Range of values at all flows	Streamwise and transverse direction (Variance)	Streamwise direction (Range)	Transverse direction (Range)	Correlation with h/k_s	
U/U_* (streamwise)	2.61 to 3.13	0.16 to 6.59	Reduced variance at high flow	Similar downstream spatial correlation length scale at both low and high flows	More variability (difficult to determine spatial correlation length scale)	• Positive correlation at both high and low flow • Relationship somewhat unclear because of presence of wood in center of channel	• Well-defined thalweg and reduced variance at high flows • Smaller values of streamwise velocity near banks at low flows
V/U_* (vertical)	0.06 to 0.14	−1.04 to 0.98	Reduced variance at high flow	Some small-scale spatial correlation at high flows, but a lack of spatial correlation at low flow	No spatial correlation	• Positive correlation at high flow • Strong negative correlation at low flow • At high flows, affect of roughness de creases with distance	• Not a strong dependence on stage in terms of spatial correlation • No cross-stream spatial dependence between points • Downwelling over break in slope and upwelling in downstream section of channel
W/U_* (cross-stream)	0.16 to 0.31	−1.97 to 1.75	Greater variance at high flow	Similar to streamwise component with a range of about 2 m at low flow and 1.6 m at high	More variability in spatial correlation length scale. Lag distance is longer at low flow.	• Positive correlation at both high and low flow	• Strong tendency for flow to move towards the left bank at high flows • Flow split at low flows with flow on the right moving towards left bank and flow on left moving towards right bank, causing convergence in center and reduced variability in streamwise direction • The range for the cross-stream velocity component is similar as the range for the streamwise velocity component in both the streamwise and transverse direction indicating that these two components have similar spatial correlation
u'/U_* (streamwise)	0.91 to 0.79	0.20 to 2.76	Greater variance at high flow; more uniform at low flow	Greater spatial correlation at high flow	Minimal correlation at high flow and no spatial correlation at low flow	• Positive and larger correlation at high flow • At high flow, spatial correlation with h/k_s decreases downstream • No significant correlation in transverse direction	• Variance is less than the variance for U/U_* • Greater correlation at high flow in the streamwise direction • At high flow, larger values in the thalweg and smaller values near the banks and at lower end of reach
v'/U_* (vertical)	1.11 to 0.88	0.20 to 4.02	Greater variance at high flow	Greater spatial correlation at high flow	Minimal spatial correlation at either stage	• Positive and larger correlation at high flow • At high flow, spatial correlation decreases downstream • No significant correlation in transverse direction	• Variance is less than the variance for V/U_* • Greater correlation at high flow in the streamwise direction • Greater values at the upstream section of stream near larger clasts • Larger values in downstream section during low flows
w'/U_* (cross-stream)	0.47 to 0.55	0.15 to 1.15	Greater variance at high flow	Greater spatial correlation at high flow	Minimal spatial correlation at either stage.	• Positive and larger correlation at high flow • At high and low flow, spatial correlation decreases downstream • No significant relationship in transverse direction	• Variance is less than the variance for W/U_* • Greater correlation at high flow in the streamwise direction • Values greatest in thalweg at high flows • Values more uniform throughout the reach at low flows

The turbulence intensity in the cross-stream direction (w'/U_*) (Fig. 11) was similar between the two discharges in terms of the mean and histogram, but the proportional symbol map and semivariograms (Fig. 12) showed some differences. During high flows, w'/U_* was greatest in the thalweg and much smaller near the banks, with a greater variance and a larger streamwise lag distance over which the points are spatially correlated. During low flows, w'/U_* was more uniform throughout the reach, resulting in a lower variance and a longer transverse range.

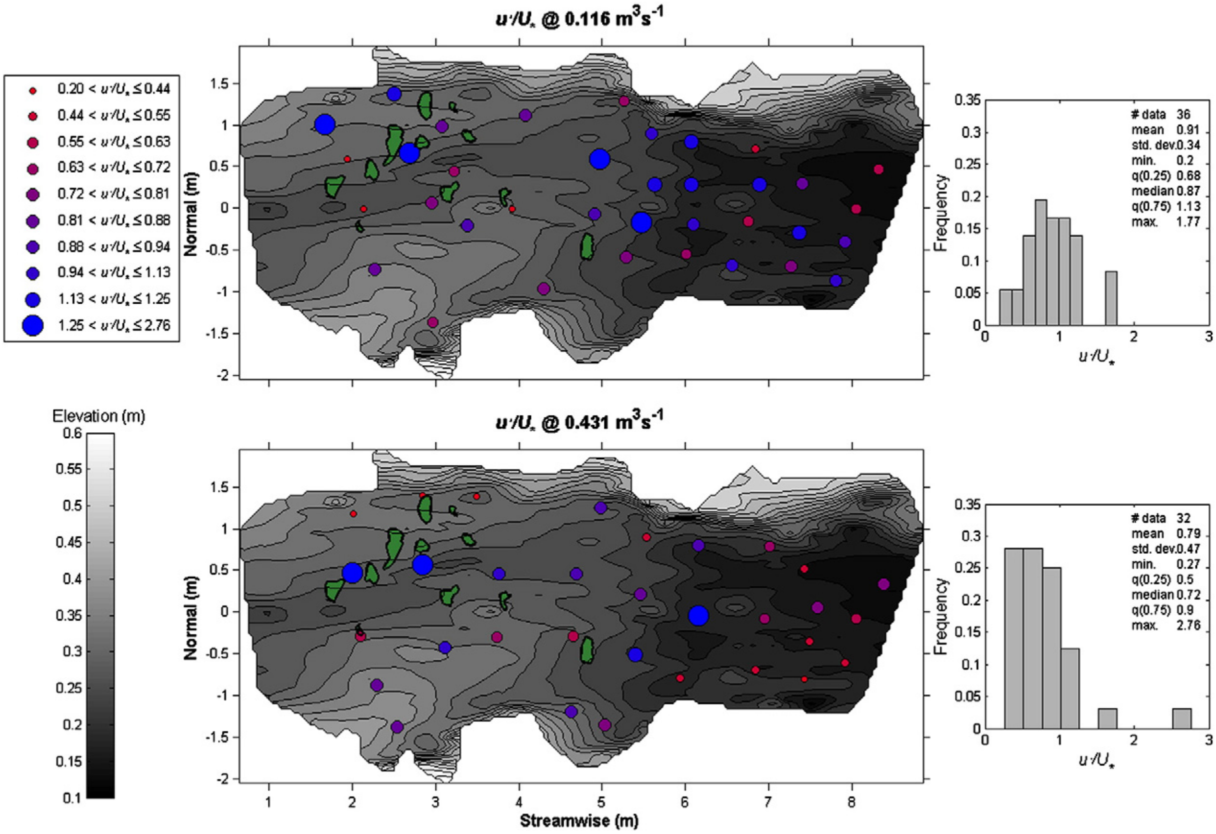

Fig. 9. Proportional symbol map and probability density histogram of non-dimensional streamwise turbulence intensity u'/U_* for each discharge.

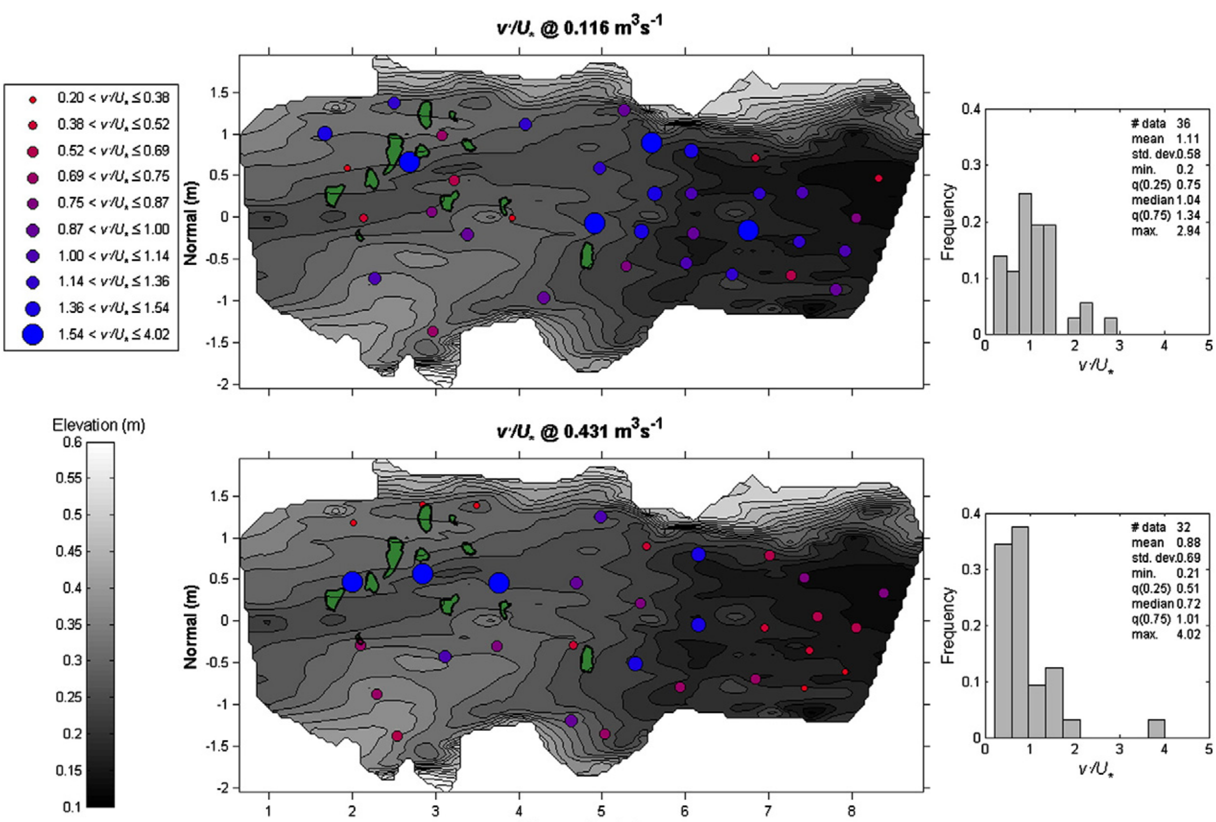

Fig. 10. Proportional symbol map and probability density histogram of non-dimensional vertical turbulence intensity v'/U_* for each discharge.

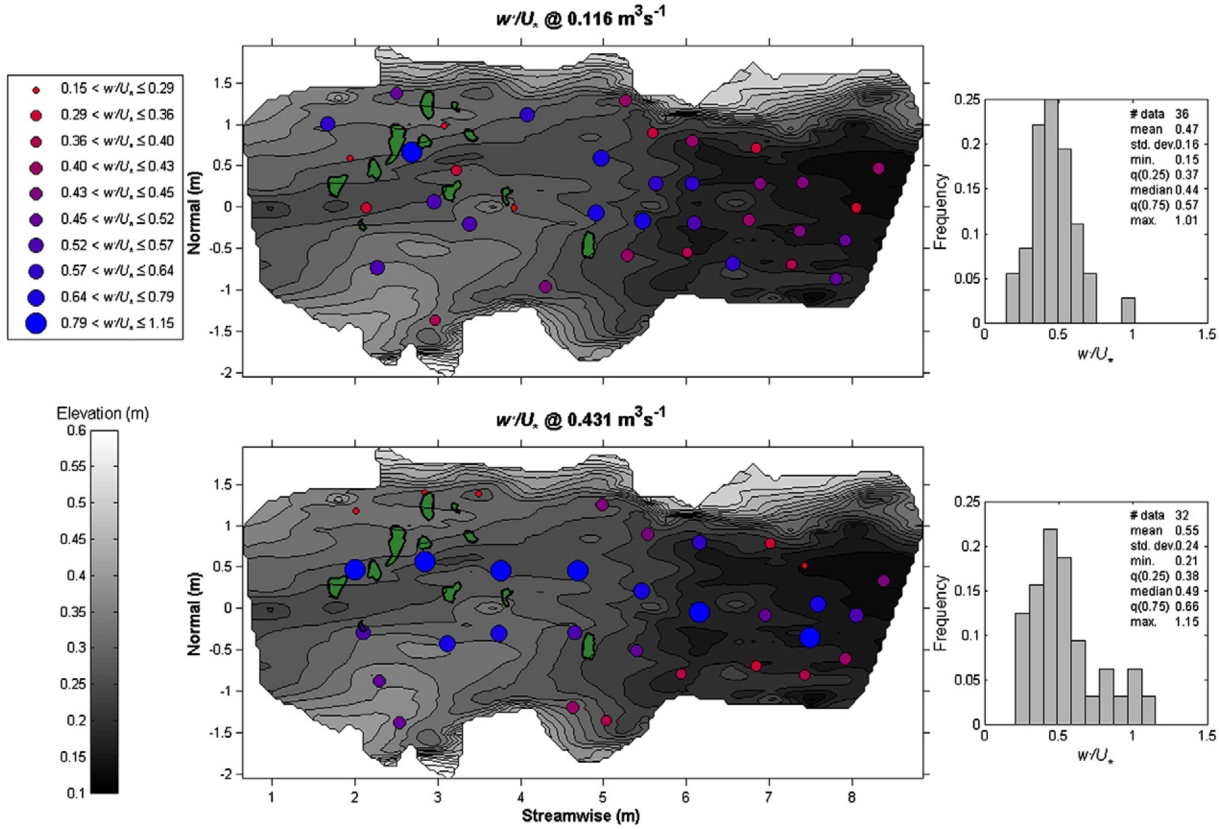

Fig. 11. Proportional symbol map and probability density histogram of non-dimensional transverse turbulence intensity w'/U_* for each discharge.

3.3. Relationship between relative submergence (h/k_s) and streamwise, vertical, and transverse velocity

The relationships between local boundary roughness, or relative submergence (h/k_s), and each of the mean velocity and turbulence intensity components in the streamwise and transverse directions are shown in Figs. 13 and 14 and summarized in Table 4. The correlation at a lag of 0 was the correlation coefficient between the flow statistic and the relative submergence at the same location. At a lag of 0, U/U_* had a similar, positive correlation with h/k_s at both high and low flow. The same was true for W/U_* and h/k_s, indicating that there was not a strong stage dependency between U/U_* and W/U_* and h/k_s. The streamwise velocity component may have had some degree of spatial correlation with h/k_s at high flow, which was interrupted by the log in the center of the channel that becomes submerged at high flows but remains above the water level at low flows. The correlation of U/U_* and W/U_* at both stages with h/k_s was positive. Therefore, where grains were more deeply submerged, the streamwise and transverse components of the mean velocity were greater.

The vertical velocity component (V/U_*) had a positive relationship with h/k_s at low flow and a strong negative relationship at high flows at lag 0, implying a stage dependency between h/k_s and V/U_*. At high flow, areas with greater relative submergence had lower vertical velocities. At low flow, areas with greater submergence had higher vertical velocities. The effect of roughness appears to decrease with distance at high flow, as shown by the decrease of the absolute value of the correlation to near zero at the first lag (Fig. 13).

The relationship between turbulence intensity and h/k_s for each component was positive and larger for the higher discharge (Fig. 14), which means that turbulence intensity was greater at higher relative submergences at high flows. The correlation between turbulence intensity components and relative submergence at the high discharge decreased with streamwise lag distance, indicating that the effect of roughness on turbulence intensity diminished downstream. On the other hand, at low flows there was not a significant streamwise spatial correlation between roughness and turbulence intensity, indicating that there was not an organized, coherent pattern to the turbulence as the flow moved downstream. There was a positive correlation at low flows between h/k_s and w'/U_*, which decreased quickly to zero in the streamwise direction. Therefore, w'/U_* was larger at higher h/k_s, but the effect of roughness on the w'/U_* was local and did not extend downstream. The relationship between any turbulence intensity component and h/k_s did not have any well-defined spatial structure in the transverse direction at either discharge.

3.4. Comparison of 3-D velocity and turbulence on plane-bed reach on ESL with step-pool and pool-riffle channels

Fig. 15 compares the non-dimensional streamwise, vertical, and transverse velocity components for the plane-bed reach against other channel types: a pool-riffle reach on the North Fork of the Cache La Poudre River (Legleiter et al., 2007), a step-pool reach in Italy on the Rio Cordon (Wilcox et al., 2011) and a step-pool reach further downstream on East St. Louis Creek (Wilcox and Wohl, 2007). The comparison was made in an attempt to understand whether changes in gross morphology resulted in significant differences between the non-dimensional velocity components. The plane-bed reach had some of the highest means and maximum values for U/U_*, along with the steps on the Rio Cordon (Fig. 15a). W/U_* had similar values for all three channel types, but there was a larger range of values for the plane-bed and pool-riffle channels. V/U_* had more of a tendency to be split between upwelling and downwelling for both the plane-bed reach and the pool-riffle channel than the step-pool channel. The streamwise turbulence intensities were highest in the

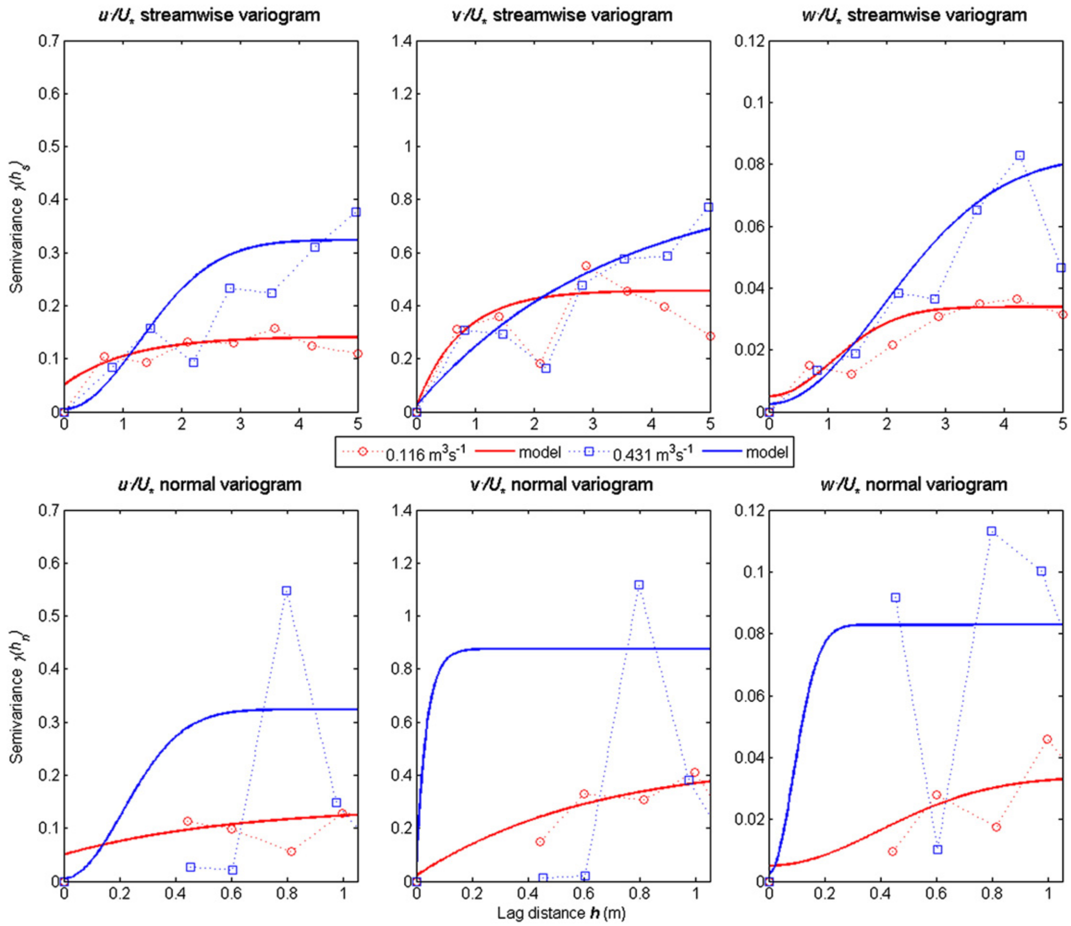

Fig. 12. Semivariograms of non-dimensional velocity in the streamwise and transverse (normal) directions at low (red/circles) and high (blue/squares) flow.

plane-bed reach, except for the turbulence intensities in the pools on East St. Louis Creek.

4. Discussion

4.1. Summary of flow characteristics at high and low flows

A spatially explicit, stochastic approach using semivariograms along with the proportional symbol maps enhanced our ability to understand flow characteristics in relation to bed topography. Using only mean velocity to describe the flow patterns in the reach does not indicate how the flow structure becomes more coherent with stage, with a defined thalweg, areas of downwelling and upwelling over small-scale bed topographic features, and significant transverse flows from the development of shear zones between fast and slow moving sections of the channel (Vermaas et al., 2011).

Flow in the plane-bed channel had a coherent structure that was primarily related to the gross morphology of the channel, rather than individual protuberant clasts, similar to the findings of Legleiter et al. (2007) and Lamarre and Roy (2005). The structure of the flow varied significantly with stage, with interrelated variations in all mean velocity and turbulence intensity components. Small bed irregularities exerted greater influence on flow structure at low flow, whereas gross channel morphology exerted a greater influence at high flow. The changing importance of different scales of channel boundary configuration as a function of flow stage supports the notion that equations for roughness need to be different for base flows versus bankfull flows (Lawless and Robert, 2001; Ferguson, 2007; David et al., 2010b, 2011; Zimmerman, 2010), whether this involves different empirical coefficients and exponents, or inclusion of some description of boundary roughness that is more spatially explicit and scale-dependent than relative submergence.

The proportional symbol maps and semivariograms indicated that at high discharge the flow is routed through the thalweg in the deeper section of the channel with a higher U/U_* (Fig. 5). The faster flow in the center of the channel created a shear zone between the thalweg and the slower flow near the banks, which resulted in a mixing layer and larger values of cross-stream flow and turbulence intensity (Figs. 7 and 11). The larger U/U_* in the thalweg was disrupted by larger protruding clasts in the upper part of the reach, which also resulted in higher values of turbulence intensity for all three components (Fig. 12). The streamwise velocity was greatly reduced around these clasts, but there was some strong downwelling and upwelling in the vertical direction and a larger transverse component that resulted in greater turbulence. At high flows, the streamwise (u'/U_*) and vertical turbulence (v'/U_*) were influenced by particular roughness elements to an extent, but these quantities also were spatially correlated over longer distances. These observations are relevant to prediction of sediment transport because our results suggest that the spatial structure of the flow field is primarily dictated by overall bed morphology and not by localized changes in the grain size or boundary roughness (σ_b). At high flows, the streamwise and transverse velocity components were generally related to the structure of the bed, with faster flow in the deeper section of channel and slower flow near the banks. The vertical velocity component had much less structure, with some connection between zones of downwelling and upwelling in the streamwise direction, but none in the transverse direction (Figs. 6 and 8). At high flows,

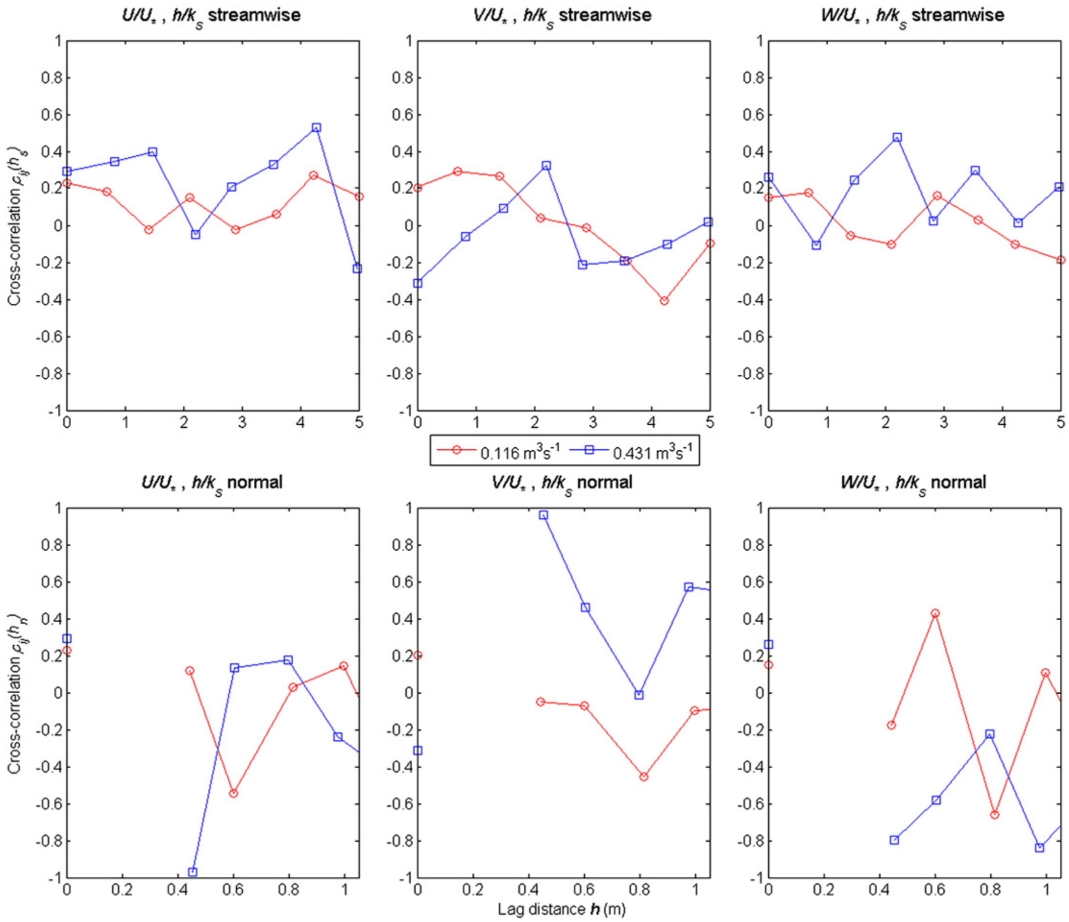

Fig. 13. Cross-correlograms of non-dimensional velocity and relative roughness in the streamwise and transverse (normal) directions at low (red/circles) and high (blue/squares) flow.

the vertical velocity downwelled over a small step in the reach and then upwelled further downstream as a result of the bed irregularity and a log (Fig. 6). Therefore, the vertical component was related to a larger-scale coherent flow structure at high flows (Roy et al., 2004), but appeared to be related to more localized roughness elements at low flows. The cross-correlograms indicated that the vertical velocity decreased at high flows as relative submergence increased and increased at low flows as relative submergence increased, implying the existence of a threshold between high and low flows where the nature of the relationship between relative submergence and vertical velocity changed. Sections of the reach with the highest vertical and transverse velocity components also had the highest turbulence. Because turbulence is connected to sediment transport, these sections presumably would have the highest sediment transport rates as well, although this was not specifically addressed in our study.

The increase in roughness at a lower stage resulted in a more uniform distribution of each velocity and turbulence intensity component. At low flow, the streamwise and vertical velocity components were more closely related to small-scale changes in the bed, which explains the increase in variance (Fig. 8). The lack of a strong streamwise component means that a distinct thalweg was not as apparent at this flow (Figs. 5 to 7). The transverse component appeared to be more closely related to a strong mixing zone between slower and faster streamwise flow (Fig. 7), and because the streamwise flow at low flow was more variable, there was not a distinct section of the channel where mixing would occur. In the lower end of the reach, flow convergence caused an increase in downwelling in the center of the channel (Fig. 6). There were also strong zones of downwelling and an increase in the streamwise velocity component as the flow moved over the small bed irregularity at meter 5. Therefore, the streamwise and vertical components seem to be more closely related to localized changes in the bed associated with grains and other small bed irregularities. The turbulence intensity at low flow was much more uniform and had a reduced range from the high flow, indicating a reduction in the degree and length scale of spatial correlation in the streamwise direction. The higher mean for the vertical turbulence intensity at low flow may be related to the bed having more of an influence at the measurement depth, because the measurement depth was closer to the bed at the lower discharge (Thompson, 2007; Hardy et al., 2011). At low flows, the turbulence intensities had very little spatial relationship with the relative submergence (Fig. 14) and only a slight positive relationship in the streamwise and vertical directions.

4.2. Comparison among plane-bed, step-pool, and pool-riffle channels

All three channel types had significant three dimensional velocity components (Fig. 15), with the streamwise component being the largest at low and high flows (Legleiter et al., 2007; Wilcox and Wohl, 2007; Wilcox et al., 2011). Patterns of flow in the plane-bed reach were mainly controlled by gross morphology, particularly at high flows in the streamwise and transverse directions, similar to the pool-riffle reach (Legleiter et al., 2007). The streamwise and turbulence intensity components were much higher for the plane-bed channel, but measured values of the transverse and vertical components fell within the same range as the other three sites. In general, plane-bed and pool-riffle channels have much lower overall flow resistance and therefore much higher

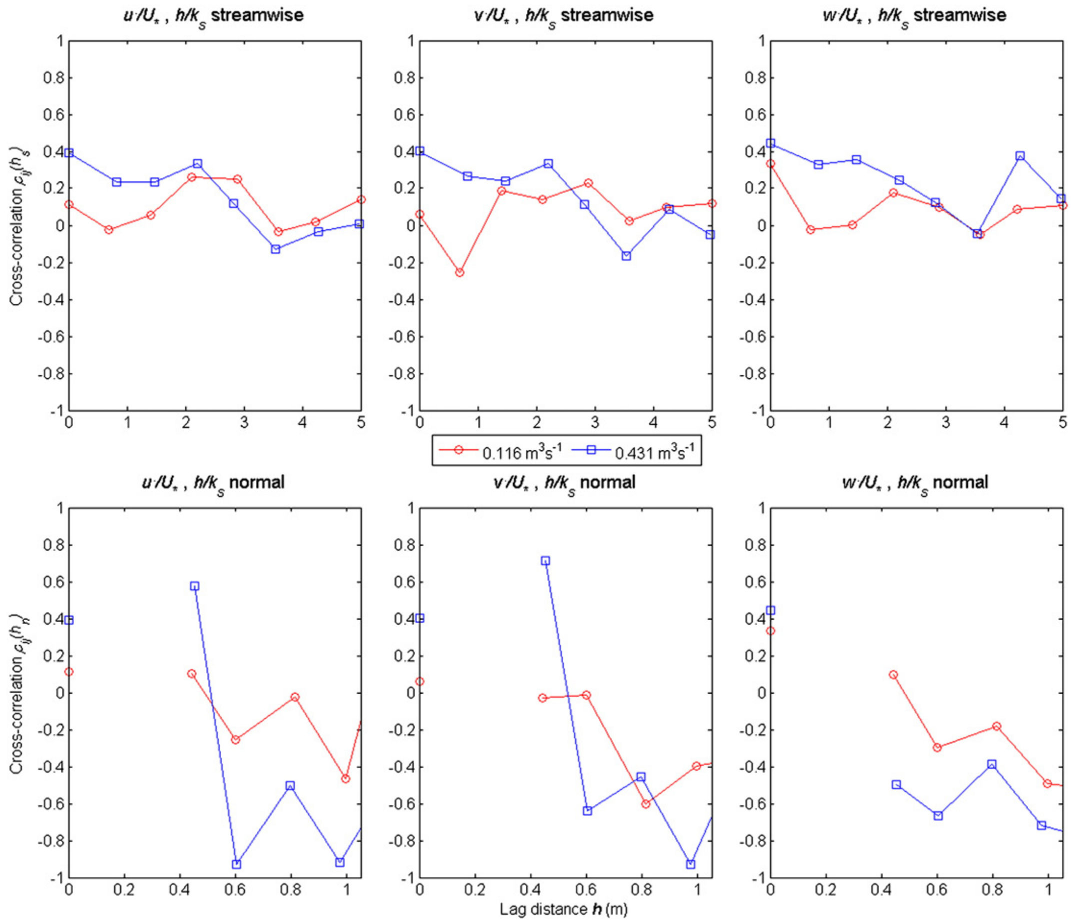

Fig. 14. Cross-correlograms of turbulence intensity and relative roughness in the streamwise and transverse (normal) directions at low (red/circles) and high (blue/squares) flow.

velocities than a step-pool reach is expected to have (David et al., 2010a, b). A step-pool reach is expected to have greater variability in velocities and turbulence because of the different morphologic characteristics of the step, step tread, and pool. As expected, the non-dimensional streamwise component was highest for the plane-bed channel, although the step section for the Rio Cordon had a similar mean and standard deviation.

The vertical component of velocity had a stronger relationship with localized variability in grains, particularly at low flows. The means and standard deviations of the vertical velocity components were all within the same range for each channel type, emphasizing the importance of variability in grains for this component. The vertical velocity component was a result of gross morphology in the step-pool channel, with flow plunging over the steps and upwelling in the pools (Wilcox and Wohl, 2007). The turbulence intensity in the vertical direction was significant in both the step-pool and plane-bed reaches, contributing at least half the total turbulence in the step-pool reach (Wilcox and Wohl, 2007). Water plunging over the step was an important component of the vertical velocity in a step-pool reach, but protuberant clasts were significant components that created similar values of vertical velocity in the plane-bed and pool-riffle channels.

Fig. 15 indicates that the transverse component was not substantially different among all three reaches, although there appears to be greater variability in the plane-bed and pool-riffle channels. The spatial structure of the turbulence intensities in the plane-bed reach was more well-defined for the streamwise direction than in Legleiter et al.'s (2007) pool-riffle reach. Similar to the pool-riffle reach, the turbulence developed a more continuous spatial structure as flow increased and the localized effects of protruding clasts were reduced. The contour maps of the plane-bed reach, however, indicate that turbulence remains high around the upstream section where there were large protruding clasts.

For all three channel types, the streamwise component was the largest and had the highest variance. The full three dimensionality of the flow was a significant component for all three channel types, even for a lower gradient plane-bed section within a high-gradient mountain system.

5. Conclusion

The geostatistical analysis of velocity in three dimensions emphasizes how the flow structure varies based on the stage, even in a plane-bed reach with only small bed irregularities. Lamarre and Roy (2005) found that complex bed topography and protuberant clasts only had minor impacts on the flow in a lower-gradient (0.002) gravel-bed river, but this variability may be important when considering sediment transport and micro-habitats for aquatic organisms. At base flows in the plane-bed reach described here, changes in grain size caused the downstream and vertical components to vary more in the streamwise and vertical directions over the entire reach, whereas the cross-stream component was less variable at low flows. The turbulence intensity was more uniform over the entire reach for all three components at low flows. Investigating velocity and turbulence in three dimensions is essential for understanding changes from base flow characterized by high variability in each component of velocity and turbulence as a result of substantial grain roughness, to high

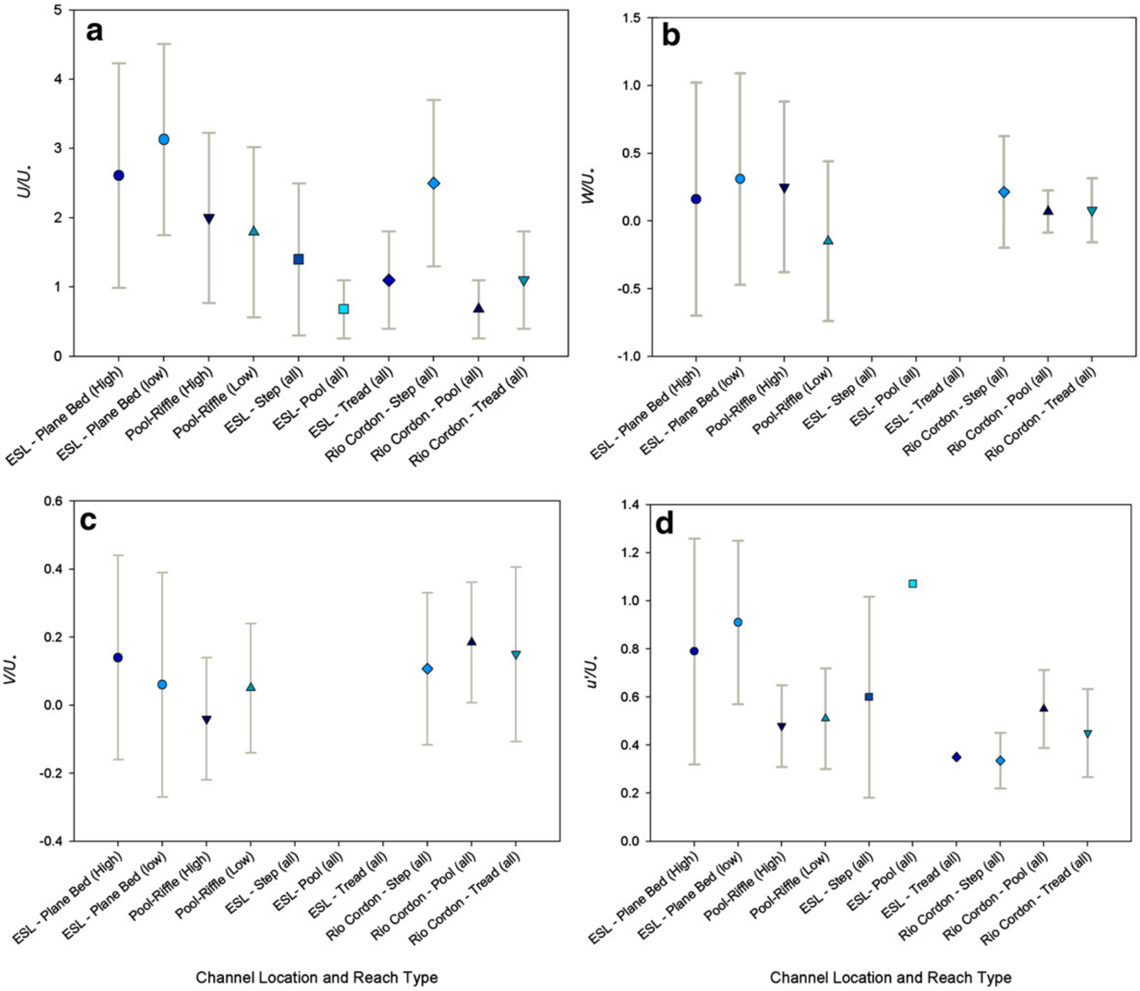

Fig. 15. The mean and standard deviation of the streamwise (a), transverse (b), and vertical (c) velocity components for the plane-bed reach in this study at low and high flow, a pool-riffle reach along the North Fork Cache la Poudre River in Colorado (Legleiter et al., 2007), a step-pool reach at ESL (Wilcox and Wohl, 2007), and a step-pool reach on the Rio Cordon in Italy (Wilcox et al., 2011). The step-pool reaches are divided up by morphologic location and summarizes the data over all flows. The streamwise turbulent intensity is shown as well (d).

flows characterized by a distinct thalweg and greater turbulence. The areas of increased turbulence were not only related to the bed morphology and protuberant clasts, but also to locations where flow converged or created shear layers, both of which tend to increase turbulence. Therefore, it is important to understand how water moving in one direction can alter the characteristics of another component of the flow. Our results indicate that spatially coherent flow structures influence turbulence intensity throughout the reach, which could also influence the development of sediment mobilizing macroturbulent events such as sweeps (Marquis and Roy, 2011). At low flow, there remains a spatial connection between streamwise and cross-stream velocity components and turbulence in the downstream direction, but turbulence became more uniform and had a less organized spatial structure. The banks appeared to have some influence on the flow, with streamwise velocities being reduced near the banks at high flow and cross-stream velocities indicating the banks deflected flow towards the middle of the channel at low flows.

Acknowledgments

This research was funded by the Hydrologic Sciences Program of the National Science Foundation (EAR 0608918). We would like to thank the USDA Forest Service Rocky Mountain Research Station and field assistants Mark Hussey, Dan Dolan, and Dan Cadol for providing logistical support. The manuscript was improved by comments from two anonymous reviewers.

References

Aberle, J., Smart, G.M., 2003. The influence of roughness structure on flow resistance on steep slopes. Journal of Hydraulic Research 41, 259–269.
Bathurst, J.C., 1993. Flow resistance through the channel network. In: Beven, K., Kirkby, M.J. (Eds.), Channel Network Hydrology. Wiley, Hoboken NJ, pp. 69–98.
Buffin-Belanger, T., Roy, A.G., 2005. 1 min in the life of a river: selecting the optimal record length for the measurement of turbulence in fluvial boundary layers. Geomorphology 68, 77–94.
Buffin-Belanger, T., Roy, A.G., Kirkbride, A.D., 2000. On large-scale flow structures in a gravel-bed river. Geomorphology 32, 417–435.
Byrd, T.C., Furbish, D.J., Warburton, J., 2000. Estimating depth-averaged velocities in rough channels. Earth Surface Processes and Landforms 25, 167–173.
Chartrand, S.M., Whiting, P.J., 2000. Alluvial architecture in headwater streams with special emphasis on step-pool topography. Earth Surface Processes and Landforms 25, 583–600.
Church, M., Zimmerman, A., 2007. Form and stability of step-pool channels: research progress. Water Resources Research 43, W03415. http://dx.doi.org/10.1029/2006WR005037.
Clifford, N.J., French, J.R., 1993. Monitoring and modelling turbulent flow: historical and contemporary perspectives. In: Clifford, N.J., French, J.R., Hardistry, J. (Eds.), Turbulence: Perspectives on Flow and Sediment Transport. Wiley, New York, pp. 1–34.
Clifford, N.J., Soar, P.J., Emery, J.C., Gurnell, A.M., Petts, G.E., 2002. Sustaining water-related ecosystems – the role of in-stream bedform design in river channel rehabilitation. Proceedings of the Fourth International FRIEND Conference held in Cape Town South Africa – Regional Hydrology: Bridging the Gap between Research and Practice, 274. IAHS Publ., pp. 407–413.

Clifford, N.J., Wright, N.G., Harvey, G., Gurnell, A.M., Harmar, O.P., Soar, P.J., 2010. Numerical modeling of river flow for ecohydraulic applications: some experiences with velocity characterization in field and simulated data. Journal of Hydraulic Engineering 136, 1033–1041.
Coleman, S.E., Nikora, V.I., Aberle, J., 2011. Interpretation of alluvial beds through bed-elevation distribution moments. Water Resources Research 47, W11505. http://dx.doi.org/10.1029/2011WR010672.
Comiti, F., Mao, L., Wilcox, A., Wohl, E.E., Mario, L.A., 2007. Field-derived relationships for flow velocity and resistance in high-gradient streams. Journal of Hydrology 340, 48–62. http://dx.doi.org/10.1016/j.jhydrol.2007.03.021.
David, G.C.L., Wohl, E., Yochum, S.E., Bledsoe, B.P., 2010a. Controls on spatial variations in flow resistance along steep mountain streams. Water Resources Research 46, W03513. http://dx.doi.org/10.1029/2009WR008134.
David, G.C.L., Wohl, E., Yochum, S.E., Bledsoe, B.P., 2010b. Controls on at-a-station hydraulic geometry in steep headwater streams, Colorado, USA. Earth Surface Processes and Landforms 35, 1820–1837. http://dx.doi.org/10.1002/esp. 2023.
David, G.C.L., Wohl, E., Yochum, S.E., Bledsoe, B.P., 2011. Comparative analysis of bed resistance partitioning in high gradient streams. Water Resources Research 47, W07507. http://dx.doi.org/10.1029/2010WR009540.
Ferguson, R.I., 2007. Flow resistance equations for gravel- and boulder-bed streams. Water Resources Research 43, W05427. http://dx.doi.org/10.1029/2006WR005422.
Ferguson, R.I., Kirkbride, A.D., Roy, A.G., 1996. Markov analysis of velocity fluctuations in gravel-bed rivers. In: Ashworth, P.J., Bennett, S.J., Best, J.L., McLelland, S.J. (Eds.), Coherent Flow Structures in Open Channels. Wiley, Chichester, pp. 165–183.
Goovaerts, P., 1997. Geostatistics for natural resource evaluation. Oxford University Press, New York. 496 pp.
Hardy, R.J., Best, J.L., Lane, S.N., Carbonneau, P.E., 2009. Coherent flow structures in a depth-limited flow over a gravel surface: the role of near-bed turbulence and influence of Reynolds number. Journal of Geophysical Research 114, F01003. http://dx.doi.org/10.1029/2007JF000970.
Hardy, R.J., Best, J.L., Parsons, D.R., Keevil, G.M., 2011. On determining the geometric and kinematic characteristics of coherent flow structures over a gravel bed: a new approach using combined PLIF-PIV. Earth Surface Processes and Landforms 36, 279–284.
Keulegan, G.H., 1938. Laws of turbulent flow in open channels. Journal of Research of the National Bureau of Standards (U.S.) 21, 707–741.
Lamarre, H., Roy, A.G., 2005. Reach scale variability of turbulent flow characteristics in a gravel-bed river. Geomorphology 68, 95–113.
Lane, S.N., Biron, P.M., Bradbrook, K.F., Butler, J.B., Chandler, J.H., Crowell, M.D., McLelland, S.J., Richards, K.S., Roy, A.G., 1998. Three-dimensional measurement of river channel flow processes using Acoustic Doppler Velocimetry. Earth Surface Processes and Landforms 23, 1247–1267.
Lawless, M., Robert, A., 2001. Scales of boundary resistance in coarse-grained channels: turbulent velocity profiles and implications. Geomorphology 39, 221–238.
Lee, A.J., Ferguson, R.I., 2002. Velocity and flow resistance in step-pool streams. Geomorphology 46, 59–71. http://dx.doi.org/10.1029/2001WR000817.
Legleiter, C.J., Kyriakidis, P.C., 2008. Spatial prediction of river channel topography by kriging. Earth Surface Processes and Landforms 33, 841–867. http://dx.doi.org/10.1002/esp. 1579.
Legleiter, C.J., Phelps, T.L., Wohl, E.E., 2007. Geostatistical analysis of the effects of stage and roughness on reach-scale spatial patterns of velocity and turbulence intensity. Geomorphology 83, 322–345.
Leopold, L.B., Bagnold, R.A., Wolman, M.G., Brush Jr., L.M., 1960. Flow resistance in sinuous or irregular channels. U.S. Geological Survey Professional Paper 282-D, pp. 111–134.
MacVicar, B.J., Roy, A.G., 2007. Hydrodynamics of a forced riffle pool in a gravel bed river: 1. mean velocity and turbulence intensity. Water Resources Research 43, W12401. http://dx.doi.org/10.1029/2006WR005272.
Marchildon, M.A., Annable, W.K., Imhof, J.G., Power, M., 2011. A high-resolution hydrodynamic investigation of brown trout (*Salmo Trutta*) and rainbow trout (*Oncorhynchus Mykiss*) redds. River Research and Applications 27, 345–359. http://dx.doi.org/10.1002/rra.1362.
Marquis, G.A., Roy, A.G., 2011. Bridging the gap between turbulence and larger scales of flow motions in rivers. Earth Surface Processes and Landforms 36, 563–568. http://dx.doi.org/10.1002/esp. 2131.
McLean, S.R., Nelson, J.M., Wolfe, S.R., 1994. Turbulence structure over two-dimensional bed forms: implications for sediment transport. Journal of Geophysical Research 99, 12,729–12,747.
Montgomery, D.R., Buffington, J.M., 1997. Channel-reach morphology in mountain drainage basins. Geological Society of America Bulletin 109, 596–611.
Nelson, J.M., Shreve, R.L., McLean, S.R., Drake, T.G., 1995. Role of near-bed turbulence structure in bed load transport and bed form mechanics. Water Resources Research 31, 2071–2086.
Nelson, J.M., Schmeeckle, M.W., Shreve, R.L., 2001. Turbulence and particle entrainment. In: Mosley, M.P. (Ed.), Gravel Bed Rivers V. Water Resources Publications, LLC., pp. 221–248.
Noss, C., Salzmann, T., Storchenegger, I., 2010. Turbulent and advective momentum fluxes in streams. Water Resources Research 46, W12518. http://dx.doi.org/10.1029/2010WR009297.
Reid, D.E., Hickin, E.J., 2008. Flow resistance in steep mountain streams. Earth Surface Processes and Landforms 33, 2211–2240. http://dx.doi.org/10.1002/esp. 1682.
Rhoads, B.L., Schwartz, J.S., Porter, S., 2003. Stream geomorphology, bank vegetation, and three-dimensional habitat hydraulics for fish in midwestern agricultural streams. Water Resources Research 39, 1218. http://dx.doi.org/10.1029/2003WR002294.
Roy, A.G., Biron, P.M., Buffin-Belanger, T., Levasseur, M., 1999. Combined visual and quantitative techniques in the study of natural turbulent flows. Water Resources Research 35, 871–877.
Roy, A.G., Buffin-Belanger, T., Lamarre, H., Kirkbride, A.D., 2004. Size, shape and dynamics of large-scale turbulent flow structures in a gravel-bed river. Journal of Fluid Mechanics 500, 1–27.
Shvidchenko, A., Pender, G., 2001. Macroturbulent structure of open-channel flow over gravely beds. Water Resources Research 37, 709–719. http://dx.doi.org/10.1029/2000WR900280.
SonTek, 2001. FlowTracker Handheld ADV Technical Documentation. Sontek/YSI, Inc., San Diego, CA. 126 pp.
Soulsby, R.L., 1980. Selecting record length and digitization rate for near-bed turbulence measurements. Journal of Physical Oceanography 10, 208–219.
Thompson, D.M., 2007. The characteristics of turbulence in a shear zone downstream of a channel constriction in a coarse-grained forced pool. Geomorphology 83, 199–214.
USDA Forest Service, 2009. About Fraser Experimental Forest. http://www.fs.fed.us/rm/fraser/about/index.shtml.
Vermaas, D.A., Uijttewaal, W.S.J., Hoitink, A.F.J., 2011. Lateral transfer of streamwise momentum caused by a roughness transition across a shallow channel. Water Resources Research 47, W02530. http://dx.doi.org/10.1029/2010WR010138.
Wiberg, P.L., Smith, J.D., 1991. Velocity distribution and bed roughness in high-gradient streams. Water Resources Research 23, 1471–1480.
Wilcox, A.C., Wohl, E.E., 2006. Flow resistance dynamics in step-pool stream channels: 1. Large woody debris and controls on total resistance. Water Resources Research 42, W05418. http://dx.doi.org/10.1029/2005WR004277.
Wilcox, A.C., Wohl, E.E., 2007. Field measurements of three-dimensional hydraulics in a step-pool channel. Geomorphology 83, 215–231.
Wilcox, A.C., Wohl, E.E., Comiti, F., Mao, L., 2011. Hydraulics, morphology, and energy dissipation in an alpine step-pool channel. Water Resources Research 47, W07514. http://dx.doi.org/10.1029/2010WR010192.
Wolman, M.G., 1954. A method for sampling coarse river-bed material. Transactions of the American Geophysical Union 35, 951–956.
Yochum, S.E., Bledsoe, B.P., David, G.C.L., Wohl, E., 2012. Velocity prediction in high-gradient channels. Journal of Hydrology 424–425, 84–98.
Zimmerman, A., 2010. Flow resistance in steep streams: an experimental study. Water Resources Research 46, W09536. http://dx.doi.org/10.1029/2009WR007913.
Zimmerman, A., Church, M., 2001. Channel morphology, gradient profiles and bed stresses during flood in a step-pool channel. Geomorphology 40, 311–327.